Transgenic quail to dynamically image amniote embryogenesis

David Huss [1,3], Bertrand Benazeraf[1,6], Allison Wallingford[1], Michael Filla[4], Jennifer Yang[5], Scott E. Fraser[3,5], and Rusty Lansford[1,2,5]*

[1]Department of Radiology and Developmental Neuroscience Program, Saban Research Institute, Children's Hospital Los Angeles, Los Angeles, CA 90027, USA.

[2]Keck School of Medicine, University of Southern California, Los Angeles, CA 90033, USA.

[3]Department of Biological Sciences, University of Southern California, Los Angeles, CA 90089, USA.

[4]Department of Anatomy and Cell Biology, University of Kansas Medical Center, Kansas City, Kansas 66160, USA.

[5]Division of Biology, California Institute of Technology, Pasadena, CA 94720, USA.

[6] Institut de Génétique et de Biologie Moléculaire et Cellulaire, CNRS (UMR 7104), Illkirch 67400, France.

*Corresponding author:
Rusty Lansford, Ph.D.
Children's Hospital Los Angeles
Keck School of Medicine of University of Southern California
Department of Radiology
Saban Research Institute
Developmental Neuroscience Program
4661 Sunset Blvd. MS #135
Los Angeles, CA 90027
T: (909) 285-5535
E: lansford@usc.edu

Development ● Accepted manuscript

© 2015. Published by The Company of Biologists Ltd.

Abstract

Embryogenesis is the coordinated assembly of tissues during morphogenesis by changes in individual cell behaviors and collective cell movements. Dynamic imaging, combined with quantitative analysis, are ideal for investigating fundamental questions in developmental biology involving cellular differentiation, growth control, and morphogenesis. However, a reliable amniote model system amenable to the rigors of extended, high resolution imaging and cell tracking has been lacking. To address this shortcoming, we produced a novel transgenic quail that ubiquitously expresses nuclear localized monomer cherry fluorescent protein (chFP). We characterize the expression pattern of the chFP and provide concrete examples of how Tg(PGK1:H2B-chFP) quail can be used to dynamically image and analyze key morphogenetic events during embryonic stages X to 11.

Development ● Accepted manuscript

Development ● Accepted manuscript

Introduction

It is easy to overlook that the developing embryo---biochemically, histologically, and molecularly detailed for over a century in static splendor—is undergoing constant change. Embryos are composed of many different progenitor and differentiated cells, arranged in complex three-dimensional relationships, continually undergoing both unique and collective movements. Morphogenesis, the process whereby cells reorganize in three-dimensional space to generate tissues and organs, results from a continual series of changes in cell shape, polarity, proliferation and movement. Imaging fixed embryos at a series of distinct developmental timepoints, while highly valuable, might not provide a complete depiction of these developmental processes over time and may inevitably miss important and transient changes. Capturing these changes in real time as the living embryo develops can add significantly to our understanding of complex cellular processes.

Dynamic imaging of embryo development has usually been carried out in lower vertebrates and invertebrates, but rarely in amniotes such as rodents due to the difficulties of accessing the living embryos. Avians have long been a favorite model organism of classical embryologists since the embryos are highly accessible to experimental manipulations and can be cultured artificially outside of the egg (Stern, 2005). In addition, the avian embryo is essentially a flat disc during the early events of development such as gastrulation, axis patterning and somitogenesis. These same traits make the avian embryo amenable to dynamic imaging and the technique has long been utilized by embryologists (Bortier et al., 1996; Kulesa and Fraser, 2011). Recent innovations in bioimaging techniques and technologies facilitate investigating the dynamic processes of avian embryogenesis at unprecedented spatial and temporal resolution. Specialized *ex ovo* culture techniques and computer controlled microscope mounted environmental chambers help us to meet the essential requirement of time-lapse imaging: that the embryo continues to live and function normally throughout the course of image acquisition.

Real time four-dimensional (4D, *xyzt*) imaging uniquely permits the behavioral history of individual and populations of live cells to be recorded in their natural environment with subcellular resolution (Bower et al., 2011). Performing time lapse imaging after transiently labeling a small population of cells with vital markers by the injection of dyes, virus or the electroporation of plasmid DNA has been enormously successful in fate mapping and cell lineage studies in avian embryos (Krull, 2004; Cui et al., 2006; Voiculescu et al., 2008; Bhattacharyya et al., 2008). Despite their great utility, these techniques do not allow for long-term cell fate tracking of a large number of cells as the reporter molecules are typically expressed in a only a small proportion of the targeted cells and the label may be diluted out during cell division. The ability

of an exogenous promoter to drive consistent, heritable, long-term expression of a vital marker such as a fluorescent protein in all of the cells in the embryo is the main strength of a transgenic avian as an imaging model system.

Transgenic avians that express fluorescent reporters constitutively or in a cell specific manner allow for the direct imaging of a large number of cellular behaviors including tissue assembly and differentiation. Over the past several years a number of transgenic chicken lines have been produced using eGFP as the marker for the transgene driven by strong ubiquitous promoters such as CMV, RSV, PGK and CAG (McGrew et al, 2004; Chapman et al. 2005; Koo et al., 2006; McGrew et al., 2008; Motono et al., 2010; McDonald et al., 2012; Park and Han, 2012). In addition, transgenic quail lines using cell specific promoters have allowed the dynamic imaging of particular tissue types, including endothelial cells (Sato et al. 2010) and neurons (Scott and Lois, 2005; Seidl et al., 2013). Targeting the fluorescent molecule as a fusion protein to a particular organelle such as the cell membrane (Rozbicki et al, 2015) has led to additional insights into cellular movement and shape changes during primitive streak formation. In particular, expressing the fluorescent protein in the nucleosomes of the chromatin within the cell nucleus has helped to facilitate the automated cell tracking of a large number of cells simultaneously (Sato et al., 2010). Building on the strengths of these previous transgenic avians, we set out to design a transgenic quail model that would be uniquely useful for the dynamic imaging and quantitative cell tracking analysis of early embryogenesis.

Here we report the development and characterization of this novel transgenic quail that ubiquitously expresses a nuclear localized red fluorescent protein, monomer Cherry (chFP), along with the imaging approaches used to record the dynamic events of early amniote embryogenesis. This transgenic line affords excellent visual access to the many cellular behaviors and morphogenetic events of embryogenesis beginning in the un-incubated blastoderm (stage X) and continuing through developmental stage 11. We detail the use of several dynamic microscopy approaches including multispectral 4D imaging and quantitative analysis to demonstrate the utility of fluorescent transgenic quail embryos in visualizing several complex morphogenetic events during early avian embryogenesis including gastrulation, head fold process formation, head patterning, and dorsal aortae formation.

Development ● Accepted manuscript

Development ● Accepted manuscript

Results

Generation of PGK1:H2B-chFP transgenic quail line

We have engineered a novel transgenic quail line that ubiquitously expresses histone 2B-mCherry fluorescent protein (H2B-chFP) under the control of the human phosphoglycerate kinase 1 promoter (PGK1). The PGK1 promoter controls transcription of the glycolytic enzyme phosphoglycerate kinase 1. We used a self-inactivating, replication-defective HIV-based lentivirus to infect and deliver the PGK1:H2B-chFP transgene (Fig.1A) into the genomes of stage X epiblastic germ cells. At 8 weeks post hatch, chimeric founders were bred with age matched wild type quail to obtain germline transmission of the PGK1:H2B-chFP transgene. Given the ubiquitous nature of the glycolytic pathway, we assumed that the Tg(PGK1:H2B-chFP) positive offspring would express the transgene in the chorioallantoic membrane (CAM) remaining in the eggshell after hatching. This was indeed the case and facilitated screening for transgenic founder lines using an epifluorescence stereomicroscope (Fig.S1). Southern blot analysis of genomic DNA obtained from the CAM tissue of putative transgenic quail offspring confirmed the generation of three independent transgenic quail lines (Q1-3) that each contained a single copy of the transgene (Fig.S2). All three Tg(PGK1:H2B-chFP) quail lines ubiquitously expressed H2B-chFP at roughly similar expression levels as determined in images collected by epifluorescence microscopy (data not shown). We chose line Tg(PGK1:H2B-chFP)1Rla (Q1) to further characterize since the chFP was more highly expressed than in the other two lines allowing the minimal amount of laser power to be used during live imaging, thus limiting any phototoxicity effects. H2B-chFP is well tolerated by the quail as evidenced by the stable propagation of the transgenic line for over 10 generations.

Tg(PGK1:H2B-chFP) quail ubiquitously express H2B-chFP during developmental stages X-11

To confirm that Tg(PGK1:H2B-chFP) embryos ubiquitously express H2B-chFP from developmental stages X-11 (Ainsworth et al., 2010; Eyal-Giladi and Kochav, 1976; Hamburger and Hamilton, 1951), we fixed the embryos at various stages, counterstained the embryos with DAPI (4',6-diamidino-2-phenylindole) to label all the cell nuclei, and imaged the embryos in 3D (xyz) by confocal and two-photon microscopy. Representative images of whole mount embryos and high-resolution sections from stages X, 2, 5, 8, and 11 are shown (Fig.1 and Fig.S3-S7). We identified and counted chFP+/DAPI+ nuclei both manually and with cell counting Imaris (Bitplane, Zurich, Switzerland) software. Few if any cell nuclei were found that were DAPI+/chFP- in the embryonic cells of developmental stages X to 11.

Heterogeneity in H2B-chFP expression linked to cell proliferation rates

We noticed that different cells and tissues within embryos of the Tg(PGK1:H2B-chFP) lines display distinct yet reproducible H2B-chFP fluorescence levels from developmental stages X-11 (Fig.1B-G and Figs.S4-6). To determine if the heterogeneous intensities of H2B-chFP fluorescence within cell nuclei correlates with DNA content as the cell passes through cell cycle stages G1-S-G2, we examined the Tg(PGK1:H2B-chFP) embryos stained with DAPI at various developmental stages. DAPI interacts stoichiometrically with A-T rich regions of DNA and thus can be used as a fluorescent gauge for the DNA content within cells in various stages of the cell cycle (Crissman and Hirons, 1994). Contrary to our expectations, the chFP^{+} and DAPI relative fluorescence intensities did not correlate within the nuclei of Tg(PGK1:H2B-chFP) embryos (arrows in Fig.1F, Fig.S3D and Fig.S4E-F), suggesting that heterogeneity in H2B-chFP^{+} fluorescence intensity does not simply result from the expected changes in DNA content resulting from DNA replication.

We hypothesized that the tissue-specific differences in chFP relative fluorescence could be due to differences in cell cycle length. Indeed in transgenic mouse models it has been observed that FPs linked to H2B tend to accumulate in the nuclei of cells which have a slower proliferation rate (Tumbar et al., 2004). To test this hypothesis we quantified the proliferation rate of embryonic cells in different tissues using 6-hour EdU (5-ethynyl-2′-deoxyuridine) incorporation and compared the cellular proliferation rates to the chFP intensities of cells in each tissue. EdU is a thymidine analog that incorporates into DNA of proliferating cells during DNA replication and can be detected by coupling to small fluorescent azides that penetrate the whole mount embryonic tissue well (Salic and Mitchison, 2008). We first noted that cells within the posterior tip of the notochord, which have a low rate of EdU incorporation, exhibit higher relative fluorescence than the adjacent lateral plate mesoderm or the presomitic mesoderm (PSM), which have a higher rate of EdU incorporation (Fig.2A-F). In general we have been able to observe a robust inverse correlation between EdU incorporation rates and H2B-chFP relative fluorescence level averages for various cells and tissues (Fig.2A-G) (n=3 experiments). For instance cells in tissues with low rates of EdU incorporation, such as the extra embryonic endoderm where 20% of the cells incorporated EdU within 6 hrs, corresponded to relatively high H2B-chFP expression average of ~35,000 relative fluorescence units (RFUs) (Fig.2A-C yellow ellipses, G). On the contrary, a high rate of EdU incorporation corresponded to low levels of H2B-chFP. For instance, in the PSM, 82% of the cells incorporated EdU within 6 hrs and had an average H2B-chFP intensity of ~21,000 RFUs. (Fig.2D-F, blue ellipses, G). We defined a statistically significant inverse linear correlation between rates of cell proliferation and average chFP intensities for several embryonic tissue types (Fig.2G) (R^2=0.79, p=0.044, n=5). These results suggest that heterogeneity in H2B-chFP expression is linked to tissue proliferation rate. Therefore Tg(PGK1:H2B-chFP) transgenic

Development ● Accepted manuscript

quail embryos can be used as a tissue proliferation reporter to dynamically determine the growth potential of embryonic territories.

Dynamic analysis of morphogenesis in living embryos

Movie 1 displays the use of 4D (*xyzt*) confocal laser microscopy to time-lapse record a Tg(PGK1:H2B-chFP) quail embryo maturing from developmental stages 3-8 with a montage of images taken approximately every 15 minutes for 16.5 hrs. The gastrulating embryo elongates along the A-P axis as converging epiblast cells intercalate along the midline to form the primitive streak (PS) (~3:00:00 time point). The head fold process begins (~5:30:00) concomitant with continued A-P elongation along the midline PS. Somites 1 begin to form bilateral and adjacent to the PS (~8:30:00) and continue until the movie ends at the 4 somite stage (16:30:00). 4D imaging permits individual cells to be tracked over time and *z*-layer. For example, Movie 2 focuses on the head fold process apparent within Movie 1 with higher spatial resolution. Movie 2 is a maximum intensity projection of the head fold process showing elongation along the A-P axis as converging epiblast cells intercalate along the midline thrusting the primitive streak and adjacent tissue anterior. At this point during development the flat trilaminar embryonic disk begins to form into a 3D embryo. Three distinct morphogenetic events can be seen occurring concurrently in Movie 2A: 1) The anterior most tissue of the embryo folds ventrally as a distinct tissue layer and descends in the posterior direction; 2) As the ventral tissue moves posteriorly, the adjacent lateral tissue simultaneously folds toward the midline to form the anterior intestinal portal (AIP); and 3) The primitive streak and Node regress posteriorly, while in the anterior part of the elongating embryo, the notochord and neural tube form and extend along the A-P axis. They are displaced dorsally as the dorsal-ventral axis thickens. Cell tracking software was used to quantitatively analyze and visualize the movement of individual cells. White 'dragon tails' showing the direction and speed of migration of individual tracked cells for the previous four time points (60 minutes) were superimposed upon the image set of the embryos (Movie 2B). Movie 2C and 2D similarly exhibit the spatiotemporal location and speed of migrating embryonic cells and are color coded to better visualize movement along the *y*-axis for the previous four time points (60 minutes). To acquire a global view of cell and tissue movements during embryogenesis, we also used wide-field epifluorescence imaging and a whole yolk, *ex ovo* avian embryo culturing method (Czirok et al., 2002). This combination permits the embryo to be observed for up to 2.5 days since the low level of applied light does not harm the living embryo. Time-lapse epifluorescence microscopy was used to image a Tg(PGK1:H2B-chFP) quail embryo from developmental stages 3 to 11 with images taken approximately every 10 minutes for 20 hrs (of 48 hours) (Movie 3, Fig.S5). Taken together, movies 1-3 indicate that living Tg(PGK1:H2B-chFP) quail embryos are able to withstand the rigors of long-term fluorescence video microscopy during gastrulation, thus providing a novel

Development ● Accepted manuscript

model organism to dynamically analyze embryogenesis in amniotes with a spatiotemporal resolution that permits cell movements to be individually and collectively analyzed using statistical approaches that yield quantitative data.

Cell proliferation and migration during head morphogenesis

Head development is a complex process that involves the assembly and integration of distinct cell and tissue types. The cranial neural folds fuse to form the presumptive ectoderm, neural tube, and neural crest while enveloped with an ectoderm layer that together will form the developing head. Cranial neural crest (CNC) cells and paraxial mesoderm in the middle of the embryo (Noden and Trainor, 2005) produce the craniofacial mesenchyme that differentiates into the cartilage, bone, cranial neurons, glia, and connective tissues of the face. In order to understand the cellular dynamics of early head formation, Tg(PGK1:H2B-chFP) quail embryos were video recorded from the dorsal perspective using 4D confocal microscopy from stages 8-10 (Movies 4-6). High-resolution static confocal microscopy confirms that the ectoderm and mesoderm derived cells within developing head region are $chFP^+$ (Fig.1D, E, 3, S5). The 4D rendering of Tg(PGK1:H2B-chFP) head formation shows the stage 8 embryo elongating along the A-P axis (Movies 1,4). It is difficult to distinguish the individual and collective cell movements in the more ventral z-sections since all $chFP^+$ cells are similarly excited with the 561 nm laser, causing a cherry emission haze from out of focus cells. To obtain better cell and tissue resolution, we analyzed individual and action grouped *z*-sections (Movie 5) which were then color-coded for further visual discrimination (Movie 6).

The single layer of ectoderm cells that envelopes the dorsal head region of the embryo were collected in layers z1-z2 along the midline and in additional z layers on the lateral periphery since the embryonic head is curved (Movie 5A). The ectoderm cells (~42 cells/100 um^2) show minimal autonomous cell movements and few neighbor-neighbor positional changes except after mitosis, thus acting and moving collectively as an epithelial sheet. The epithelial cells are actively dividing, but there is no apparent coordination in their cell cycle or orientation of cell division (Movie 5A,B).

Confocal layers z3-z7 visually captured the mesencephalic neural crest (NC) cells as they delaminate from the neural tube (NT) via epithelial-mesenchymal transformations and migrate en masse bidirectionally and dorsolaterally along the curved basal side of the non-neural ectoderm cells into anatomical territories rich in mesodermal cells (Movies 5C,D and 6A-D; Fig.3B). The CNCs move ~200 µm in 10 hrs or about 20 µm/hr. The migrating CNCs show limited cell proliferation, possibly tempered by their strong lateral migration. The head mesenchyme cells which can be seen ventral and lateral to the NT move randomly and independent of one another, while occasionally undergoing cell divisions within the cavity (Movie 5E). Finally, the entire NT

Development ● Accepted manuscript

extends ventrally beyond the ideal resolving power of the laser microscope (~75 um). The cell density of the NT is too high to dynamically resolve the individual cells with the microscope settings used. However, it is possible to see NT morphogenesis at the tissue level (Movie 5E and 6). The confocal layer z14 movie segment focuses on the NT as it moves anterior and presses against the anterior most ectoderm cells, flattening and then bifurcating laterally to form the optic vesicles. Thus, the distinct movements of the various cell populations involved in stage 8-10 head formation can be readily visualized, resolved, and analyzed within multiple independent *z*-layers. The directed migration of the CNCs stands in contrast to the ballooning expansion of the embryo enveloping ectoderm, the sparse and randomly moving head mesenchyme, and the anterior surging neural tube.

Multispectral dynamic analysis of aortic vasculogenesis

Vasculogenesis, the de novo assembly of blood vessels, involves changes in cell proliferation, differentiation and morphogenesis. The Tg(PGK1:H2B-chFP) and Tg(TIE1:H2B-eYFP) quail lines were interbred to produce stable Tg(PGK1:H2B-chFP; TIE1:H2B-eYFP) transgenic lines to study the events of vascular development. The TIE1:H2B-eYFP transgene marks endothelial cells (ECs) with nuclear localized eYFP (Sato et al., 2010). The Tg(PGK1:H2B-chFP; TIE1:H2B-eYFP) double transgenic quail embryos permit all cells, including the putative angioblasts (defined here as $chFP^{+}/YFP^{-}$ nuclei that soon are $chFP^{+}/YFP^{+}$ nuclei), to be tracked by multispectral 4D imaging in the red channel and the ECs and endocardial cells to be separately identified and tracked in the yellow channel.

As a proof of concept, we dynamically imaged dorsal aortae assembly using Tg(PGK1:H2B-chFP; TIE1:H2B-eYFP) embryos at embryonic stages 6-11. A representative time-lapse movie shows the assembly by vasculogenesis of adjacent dorsal aortae (Movie 7). Initially, mesoderm cells proliferate and differentiate into angioblasts (Movie 7 and Fig.5). Similarly, the putative angioblasts appear to proliferate and differentiate into ECs, interact and assemble into blood vessels that soon form lumens to permit blood flow and vascular networks to enable circulation (Movies 7-9). Putative angioblasts ($chFP^{+}/YFP^{-}$) can be seen interacting in the extra embryonic vascular plexus as they proliferate, differentiate into ECs ($chFP^{+}/YFP^{+}$) within minutes of one another, and migrate to self-assemble the primary vascular plexus (Movies 7-10). The aortic ECs cells appear to move quasi collectively, since they are seen changing their neighbor-neighbor relations, yet are moving en masse in the same anterior direction (Movie 10). The metaphase plate of dividing aortic ECs shows no obvious preferred orientation, which likely accounts for the concurrent increase in length and girth of the aortae at these developmental stages (Zeng et al., 2007). ECs from the adjacent vascular plexus can be seen streaming medially into ventral half of the dorsal aortae, and toward the forming heart atria just above the descending AIP. It is readily

Development ● Accepted manuscript

apparent that the forming dorsal aortae, notochord, vascular plexus, and somites are independently moving in the anterior direction at the region of the trunk that we are viewing as the embryo elongates along the A-P axis (Movie 7-9). However, we appreciate that the observed anterior movement is transient and stalls or changes directions as the embryo matures (Movies 1 and 2). The example of dorsal aortae formation visualized by multispectral 4D imaging of Tg(PGK1:H2B-chFP; TIE1:H2B-eYFP) embryos shows the seamless interplay of cells displaying distinct and overlapping behaviors that drive transient tissue assembly processes.

Conclusion

Tg(PGK1:H2B-chFP) quail permit dynamic investigations of morphogenetic processes

Many tools in developmental biology acquire static information to investigate the transient processes of the living embryo. It is our contention that to understand the actual physiological state of a cell or tissue, it must be studied within the multicellular environment in which it evolved, the living embryo. Transgenic quail are amenable to the rigors imposed by vital imaging and have sufficient optical transparency to record and study individual and collective cell behaviors *in vivo*. Multiple time-lapse movies demonstrate how various embryonic cells and tissues within living Tg(PGK1:H2B-chFP) embryos can be recorded and studied using vital imaging to examine transient developmental events such as gastrulation (Movies 1-3), neural development (Movies 1-6), and vascular development (Movies 7-10) with subcellular resolution. We showed for the first time in an amniote that the distinct movements of the three germ layers (endoderm, mesoderm and ectoderm) can be visualized, resolved, and analyzed within multiple independent z layers (Movies 4-6). By crossing two independent transgenic quail lines we generated Tg(PGK1:H2B-chFP; TIE1:H2B-eYFP) double positive embryos to highlight the potential of multispectral 4D imaging of living embryos.

The nuclear localized fluorescent protein of the Tg(PGK1:H2B-chFP) quail permits most cells to be recorded and distinguished from neighboring cells, since the cytosol surrounding the nucleus is unlabeled. This in turn allows for the use of automated image analysis software to segment and track embryonic cells *in vivo,* greatly facilitating the laborious task of quantitative analysis of hundreds to thousands of cells within whole embryos across multiple time points (Kanda et al., 1998; Sato et al., 2010).

Development ● Accepted manuscript

Development ● Accepted manuscript

Tg(PGK1:H2B-chFP) acts as a dynamic reporter of cell proliferation

While the cellular expression of H2B-chFP is ubiquitous, the relative fluorescence intensity of chFP in individual cells and tissues is heterogeneous when viewed across time and space (Fig.1,2, S4-6). We observed that cells within the posterior tip of the notochord and extra embryonic putative endoderm cells that incorporated EdU at a low rate, also exhibited higher relative fluorescence than other tissues that proliferate more rapidly (Fig.2). These data indicate that the Tg(PGK1:H2B-chFP) transgenic quail embryo is a reliable reporter of proliferation rate (Fig. 2). The observed cellular variability in H2B-chFP mean fluorescence intensities is a function of the transgene or the transgene's expressed cargo and not the transgene's copy number or chromosomal integration site since all three transgenic lines contain a single transgene and a unique chromosomal integration site (Feng et al., 2000). These results suggest that H2B-chFP accumulates in cells that proliferate slowly and gets diluted out in cells that proliferate rapidly. Other studies have shown transiently expressed H2B-GFP reporters accumulate and dilute as a function of the cellular proliferation rate in mouse models, and thus provide a precise quantitative proliferation history of a cell and tissue (Foudi et al., 2009; Tumbar et al., 2004). It is well known that post-translational modifications of H2B regulate many processes within the nucleus including transcription initiation and elongation, silencing, and DNA repair (Weake and Workman, 2008). It may be that the expression of H2B-chFP is based on the regulation of the PGK1 promoter region, the expressed transcript, or H2B-chFP protein due to chromatin interactions or post-translational modifications of histone 2B. While the exact molecular mechanism for this observation will require addition studies, the heterogeneity of chFP expression in Tg(PGK1:H2B-chFP) quail should help us better understand how cell proliferation rates contribute to the differential growth of various tissues and regions during early embryogenesis (Ridenour et al., 2012; Sakaue-Sawano et al., 2008).

Transgenic avians are providing new tools for a classical model system

The Tg(PGK1:H2B-chFP) quail adds to an ever-growing list of transgenic avians generated over the past decade in quail (Sato et al., 2010; Scott and Lois, 2005; Seidl et al., 2013), chicken (Balic et al., 2014; Chapman et al., 2005; McGrew et al., 2004; McGrew et., 2008: Motono et al., 2010; Rozbicki et al., 2015), and songbird (Agate et al., 2009) that express reporter proteins in a ubiquitous or tissue-specific manner.

The traditional chick-quail chimera technique uses histological stains or immunohistochemistry to distinguish quail from chicken nucleoli in chimeric embryos for cell lineage studies (Le Douarin, 1973; Le Douarin and Barq, 1969; Le Douarin and Kalcheim, 1999). Since transgenic avians with ubiquitous promoters express their reporter proteins stably, their

tissues are excellent candidates for classical ectopic grafting experiments, using fluorescent microscopy to track cell and tissue fates over long periods of time. For example, McGrew et al. (2008) grafted cells from their CAG:eGFP transgenic chicken line into WT hosts in order to elucidate the fates of separate groups of progenitor cells within the elongating tail bud. Recently, cloacal tissue from donor GFP-transgenic chicken embryos transplanted into the hindlimb of wild-type chicken embryos demonstrated the conserved ability of some mesenchymal cells to respond to the cell signaling required for the formation of external genitalia (Tschopp et al., 2014). These works clearly demonstrate the power of the Tg chick –chick transplant technique. Likewise, since the H2B-chFP label is integral to all of the cells, does not spread to adjacent cells and will not disappear with cell proliferation, the Tg(PGK1:H2B-chFP) quail should allow transplanted cells to be easily distinguished from host cells and dynamically followed in chick-Tg quail or quail-Tg quail chimeras.

At the time of egg laying, (stage EG.X), there are ~50,000 $chFP^{+}$ cells within the area pellucida of the Tg(PGK1:H2B-chFP) blastoderm (Fig.1B-E and Fig.S3). Stable chFP expression in these cells permits early cell movements of the developing blastula and gastrula (Movie 2) to be dynamically studied starting immediately in un-incubated eggs without the need for extrinsic labels such as injected vital fluorescent dyes or transfected fluorescent protein expression vectors which typically take 1-10+ hours for the FPs to be expressed at levels sufficient for dynamic imaging (Bower et al., 2011). Dye labeling approaches may not provide single cell resolution and can fade over time due to dilution from cell divisions or from photobleaching during imaging (Bower et al., 2011; Clarke and Tickle, 1999). Electroporation into pre-stage 3 embryos is technically challenging as the embryos are very fragile and highly sensitive to the transfection procedure (Cui et al., 2006; Voiculescu et al., 2008). Electroporation in particular may introduce highly variable numbers of expression vectors per cell and thus their genetic cargo is expressed at highly variable levels, which greatly complicates image analysis (Momose et al., 1999; Nakamura et al., 2004). Despite these technical limitations, in cases where the experimental question requires the labeling of a small population of cells with extrinsic markers, the Tg(PGK1:H2B-chFP) quail embryos should prove to be very useful. The ubiquitously labeled chFP+ cells of the transgenic quail may provide the background tissue context in which the extrinsically labeled cells are moving and interacting.

Technical considerations of the Tg(PGK:H2B-chFP) model system

The standard tiled multispectral 4D whole embryo imaging experiment, as shown in Movie 7, uses confocal fluorescence microscopy to capture 50-200µm deep Z stacks every ~2-6 minutes for 6-48 hours. Two-photon laser scanning microscopy (TPLSM) in theory offers deeper imaging, reduced photo-damage from out of focus illumination, and the ability to image multiple labels in

Development ● Accepted manuscript

the same living specimen (Lansford et al., 2001) . As a proof of concept, we used TPLSM to image through the entire (~150 μm D-V) trunk region of a fixed stage 10 Tg(PGK:H2B-chFP) embryo with sub cellular *z*-resolution (Fig.S7). We found that the Tg(PGK.H2B-chFP) cells are best excited from 1040-1160 nm (data not shown), which agrees with previous reports (Drobizhev et al., 2011; Drobizhev et al., 2014; Vadakkan et al., 2009). Unfortunately, high Z resolution image acquisition requires largely overlapping *Z* stacks and therefore results in longer laser exposure. Imaging with the high laser power necessary to excite chFP with TPLSM under high *Z* resolution conditions is highly deleterious to the living embryo during time-lapse imaging (data not shown) likely due to photo damage (Drobizhev et al., 2011). We are confident that continued advances in confocal imaging platforms such as highly efficient lasers coupled with more sensitive detectors will reduce the laser power needed to excite and detect chFP thus leading to greater embryo survival during dynamic TPSLM imaging sessions.

Because of its high speed optical sectioning capabilities, light sheet microscopy can image large regions of a specimen with very high spatial and temporal resolution. This technique holds great promise for the dynamic imaging of actively developing transgenic avians. Recently, Rozbicki et al., (2015) used single photon light sheet imaging to study the large - scale tissue flows associated with primitive streak formation using a transgenic chicken ubiquitously expressing a membrane linked GFP. Because all cell nuclei are fluorescent in Tg(PGK1:H2B-chFP) quail embryos, complex tracking analysis in both mesenchyme and epithelium is made possible (movie 5). Therefore, when used in combination with new emerging microscopy techniques such as light sheet, the Tg(PGK1:H2B-chFP) quail will be an excellent amniote model system for imaging the entire embryo through multiple early developmental stages.

Development ● Accepted manuscript

Acknowledgements

We thank Charlie Little and members of the Lansford lab for critically reading the manuscript.

Competing interests

The authors declare no competing financial interests.

Author contributions

Conceived and designed the experiments: DH BB RL. Performed the experiments: DH BB AW JY MF RL. Analyzed the data: DH BB SEF RL. Wrote the paper: DH BB RL.

Development ● Accepted manuscript

Figures

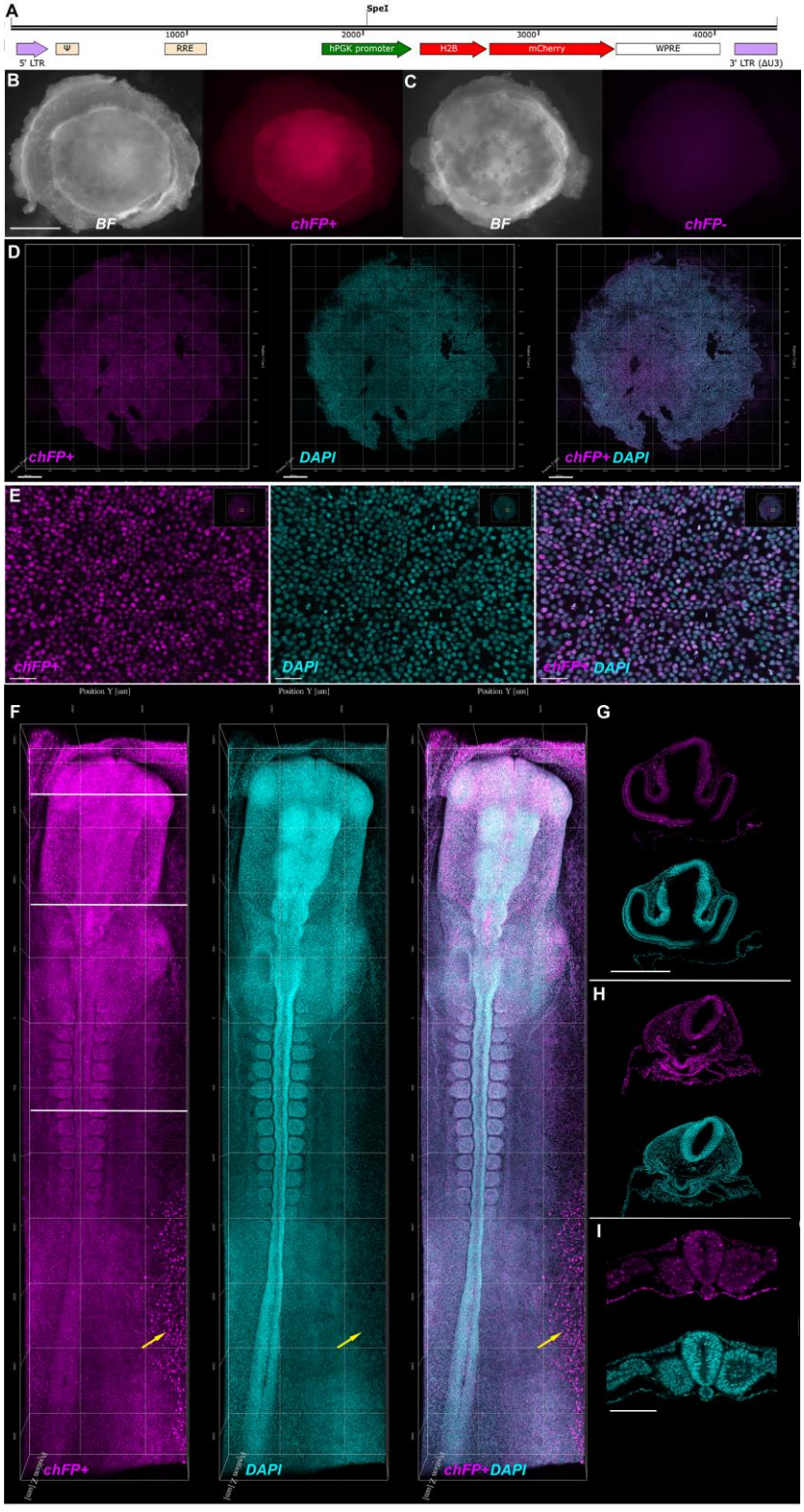

Fig.1. Characterization of developmental stage X and 11 Tg(PGK1:H2B-chFP) quail.

(A) Schematic representation of the PGK:H2B-chFP lentivector following chromosomal integration. The length of the proviral sequence from the 5' LTR to the 3' LTR is 4352bp. The SpeI restriction site used to digest the genomic DNA for Southern blotting analysis is indicated. The gray line represents the 646bp probe used during Southern analysis. LTR, long terminal

repeat; psi, packaging signal; RRE, Rev-response element; cPPT, central polypurine tract; WPRE, woodchuck hepatitis virus posttranscriptional regulatory element.

(B) Stereomicroscope acquired images of developmental stage X (un-incubated) Tg(PGK1:H2B-chFP) and (C).

wt embryo. The embryos in B and C have been isolated away from the egg yolk. BF (Brightfield). Scale bar for B and C, 1mm.

(D) Confocal images for chFP+, DAPI, and chFP+/DAPI overlay of developmental stage X Tg(PGK:H2B-chFP) wholemount quail blastoderm and (E) higher magnification images to confirm ubiquitous and heterogeneous $chFP^{+}$ expression. Variable chFP expression can be seen from cell to cell in the epiblast monolayer at stage X (Fig.1B,C) that does not directly correlate with DAPI fluorescence intensity. Scale bar D, 500um, scale bar E, 50um.

(F) Confocal images for $chFP^{+}$, DAPI, and $chFP^{+}$/DAPI overlay of developmental stage HH11 Tg(PGK:H2B-chFP) wholemount quail embryos. Some extra embryonic cells consistently display very high levels of chFP fluorescence (marked by yellow arrows). Dorsal perspective. Grid scale marked every 500 um along *xy* axes.

(G-I) Transverse vibratome section images for $chFP^{+}$ and DAPI at approximately the A-P region noted by the white lines in Fig.1F confirm ubiquitous but heterogeneous $chFP^{+}$ expression. Scale bar G-H, 500um. Scale bar I, 200um.

Development ● Accepted manuscript

Development ● Accepted manuscript

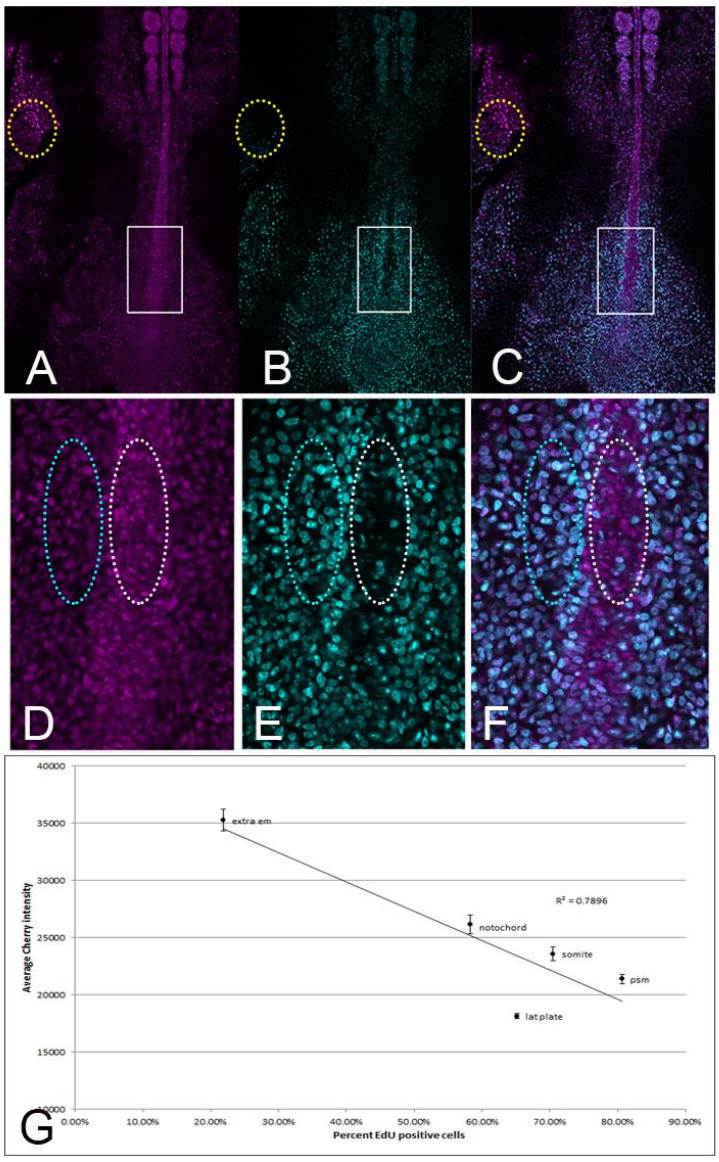

Fig.2. H2B-chFP levels correlate with cell cycle time in embryonic tissues.

(A-F) Confocal *z* slices of EdU staining (6hrs incorporation)(cyan color) and chFP fluorescence (magenta color) in the posterior part of a stage 10 Tg(PGK1:H2B-chFP) quail embryo. (A,D) chFP signal, (B,E) EdU signal. (C,F) overlay. (D,E,F) correspond to white rectangles in A,B,C; Yellow circles show low EdU /high chFP level extra embryonic endoderm. Blue ellipses show high EdU incorporation in the PSM and corresponding low chFP intensity level. White ellipses show low EdU incorporation in the posterior tip of the notochord and corresponding high chFP level. (G) A plot of the average cellular chFP intensity for different regions of the embryo compared to the percentage of EdU incorporation showing significant linear correlation (R^2=0.79, p=0.044, n=5), errors bars are standard errors of the mean. (extra em, extra embryonic endoderm; lat plate, lateral plate; psm, presomitic mesoderm).

Development ● Accepted manuscript

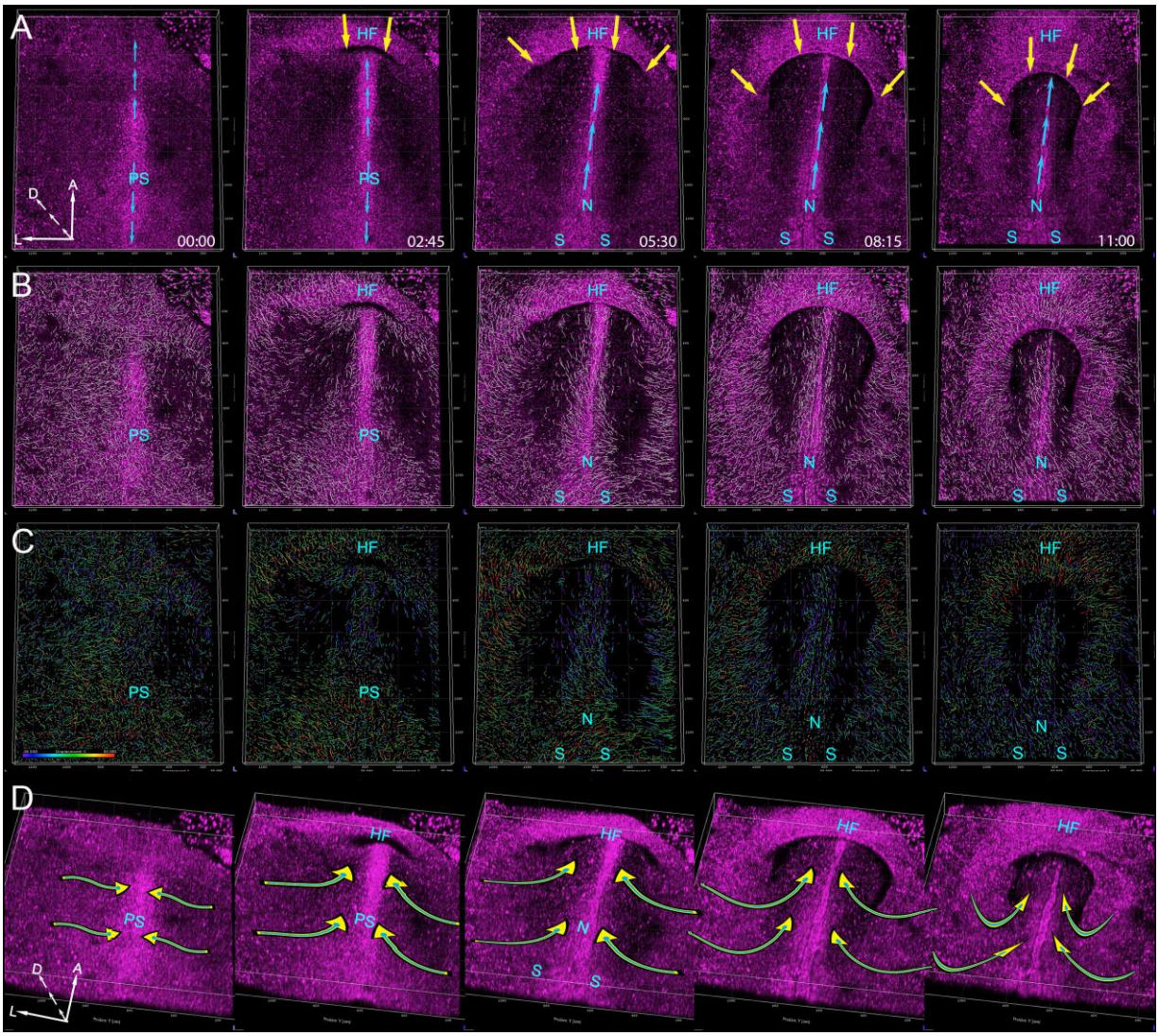

Fig.3. Representative images of time-lapse microscopy of a Tg(PGK1:H2B-chFP) embryo showing cell and tissue movements of the head fold process.

(A) Five representative images from Movie 3 of the head fold process in the gastrulating embryo, showing elongation along the A-P axis as converging epiblast cells intercalate along the midline thrusting the PS and adjacent tissue anterior until they fold ventrally and then descend in the posterior direction. As the ventral tissue moves posterior, adjacent lateral tissue simultaneously folds toward the midline to form the AIP. Cyan colored sets of three arrows highlight dorsal tissue movement along the midline in the A-P directions. Yellow colored arrows highlight ventral tissue movements of the head fold process and resulting AIP formation in the ventral and medial directions.

(B) Tracking cells to show direction and speed of migration. The cell tracks, shown as white 'dragon tails' that represent a cell's location for the previous four time points (60 minutes) are overlayed on Movie 3A.

(C) Tracking cells to indicate movement along the *y*-axis, direction, and speed of migration. The cell tracks are color-coded 'dragon tails' that represent a cell's location and movement along the *y*-

axis (-50 Anterior to 50 Posterior) for the previous four time points (60 minutes).

Lower left scale bar: 200 um; grid scale marked every 500 um along xy axes; time scale in lower right corner. PS, primitive streak; HF, head fold; N, notochord; S, somite. Skewed perspective is 130% zoom.

The representative images in (A-C) have identical time points as shown in the lower right region of the images and correspond to the time points of Movie 3. The white axes in the lower left corner of Fig.3A; A, anterior; M, medial; D, dorsal.

Development ● Accepted manuscript

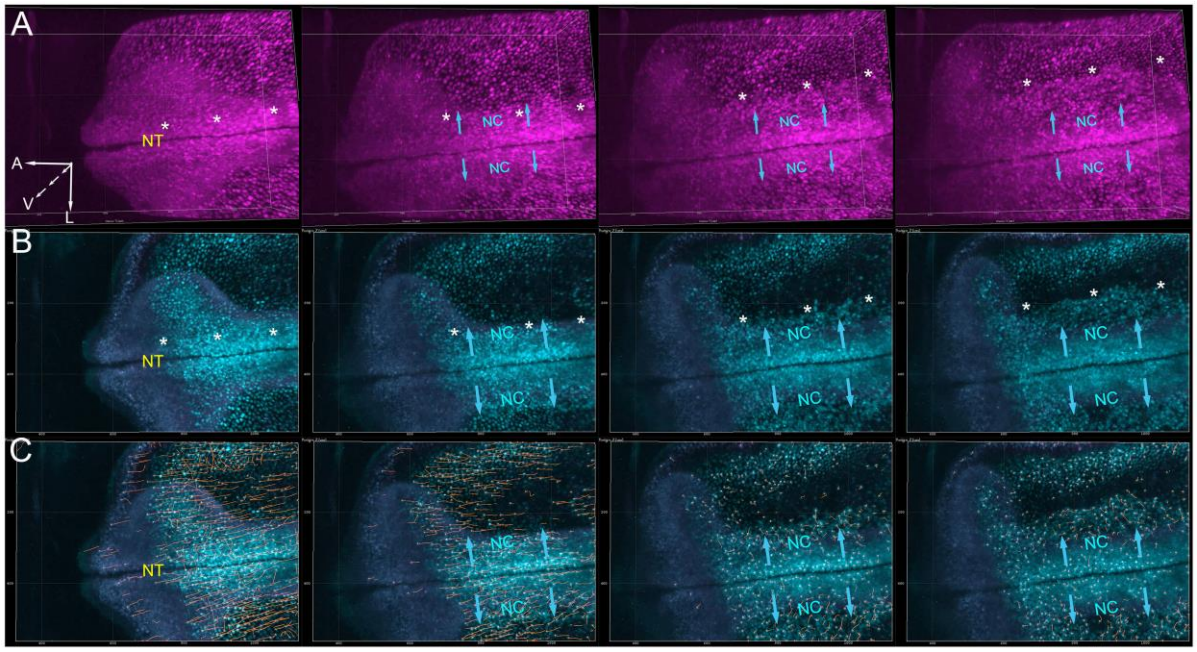

Fig.4. Distinct cell behaviors in different z layers during head formation.

(A) Representative images derived from Movie 4 of a 4D rendering of the forming head region of a Tg(PGK1:H2B-chFP) embryo at ~105 min intervals. In the first frame, the embryo is elongating along the A-P axis as it moves to the left side of the image. As the anterior movement subsides, NC cells begin to delaminate from the NT and migrate bilaterally and ventrally along the inner side of the non-neural ectoderm (leading edge of migrating NC cells is marked with white asterisks, direction of migration marked by cyan arrows) as seen in the next three frames.

(B) Z layers were distinctly pseudo-colored to better visualize the relative movements chFP^{+} cells and tissues in different z layers, (z3-7 in cyan, and z10-14 in magenta). NC cells egress from the NT and bilateral migration (marked by cyan arrows) begins, which can be viewed in Movie 6B.

(C) Tracked cells are marked by an orange 'dragon tails' to help visualize the speed and direction of individual cell movements, which can be viewed in Movie 6C.

Dorsal view. Lower left scale bar: 200 um; grid scale marked every 200 um along xy axes; A, anterior; NT, neural tube; NC, neural crest. The white axes in the lower left corner of Fig.4A; A, anterior; M, medial; V, ventral.

Development ● Accepted manuscript

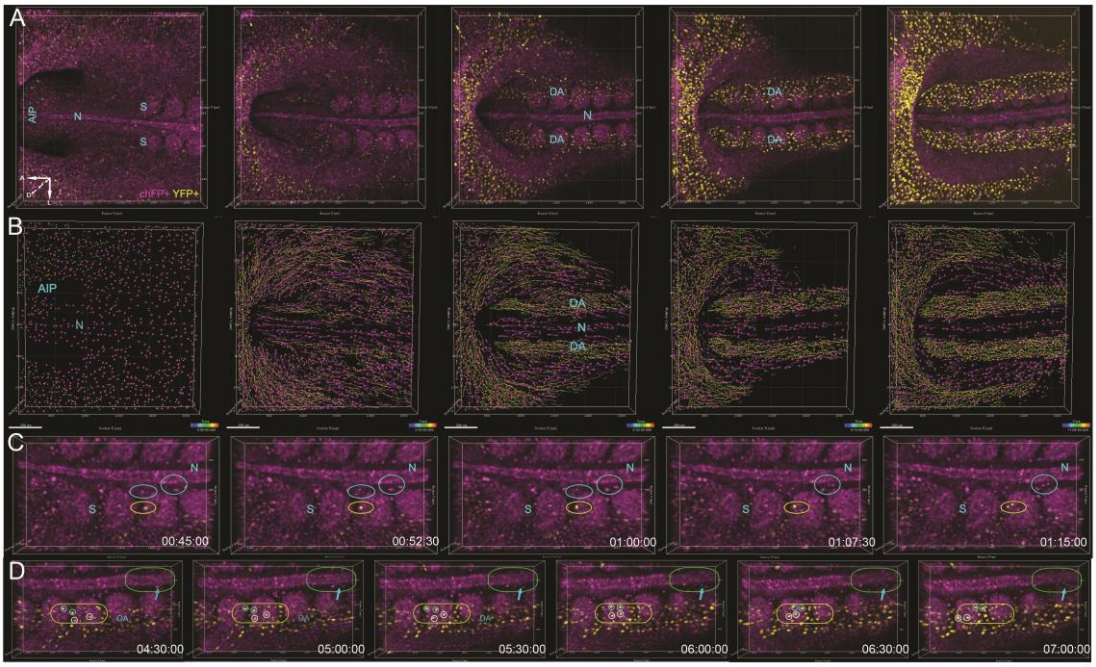

Fig.5. Representative images of multispectral 4D imaging of a Tg(PGK1:H2B-chFP; TIE1:H2B-eYFP) embryo shows assembly of dorsal aortae within the developing ventral trunk region.

(A) Representative image sequence from Movie 6 showing dorsal aortae formation in a Tg(PGK1:H2B-chFP; TIE1:H2B-eYFP) double transgenic quail embryo with chFP+ cell nuclei (magenta) and YFP^+ EC nuclei (yellow).

(B) Cell tracking data from $chFP^+/YFP^+$ cells image sets used to generate Movie 7 of Tg(PGK1:H2B-chFP; TIE1:H2B-eYFP) embryo cells.

Lower left scale bar: 150 um; grid scales mark every 200 um along *xy* axes; time scale in lower right corner; AIP, anterior intestinal portal; N, notochord; S, somite; DA, dorsal aortae. The white axes in the lower left corner of Fig.5A; A, anterior; M, medial; D, dorsal.

Development ● Accepted manuscript

Development • Accepted manuscript

References

Agate, R. J., Scott, B. B., Haripal, B., Lois, C. and Nottebohm, F. (2009). Transgenic songbirds offer an opportunity to develop a genetic model for vocal learning. *Proceedings of the National Academy of Sciences of the United States of America* **106**, 17963-17967.

Ainsworth, S. J., Stanley, R. L. and Evans, D. J. R. (2010). Developmental stages of the Japanese quail. *Journal of Anatomy* **216**, 3-15.

Balic, A., Garcia-Morales, C., Vervelde, L., Gilhooley, H., Sherman, A., Garceau, V., Gutowska, M. W., Burt, D. W., Kaiser, P., Hume, D. A., et al. (2014). Visualisation of chicken macrophages using transgenic reporter genes: insights into the development of the avian macrophage lineage. *Development* **141**, 3255-3265.

Bhattacharyya, S.,Kulesa, P.M., Fraser, S.E. (2008) Vital labeling of embryonic cells using fluorescent dyes and proteins. *Methods Cell Biol* **87**, 187-210.

Bower, D. V., Sato, Y. and Lansford, R. (2011). Dynamic lineage analysis of embryonic morphogenesis using transgenic quail and 4D multispectral imaging. *Genesis* **49**, 619-643.

Chapman, S., Collignon, J., Schoenwolf, G. C. and Lumsden, A. (2001). Improved method for chick whole-embryo culture using a filter paper carrier. *Developmental Dynamics* **220**, 284-289.

Chapman, S. C., Lawson, A., Macarthur, W. C., Wiese, R. J., Loechel, R. H., Burgos-Trinidad, M., Wakefield, J. K., Ramabhadran, R., Mauch, T. J. and Schoenwolf, G. C. (2005). Ubiquitous GFP expression in transgenic chickens using a lentiviral vector. *Development* **132**, 935-940.

Clarke, J. D. W. and Tickle, C. (1999). Fate maps old and new. *Nat Cell Biol* **1**, E103-E109.

Crissman, H. A. and Hirons, G. T. (1994). Staining of DNA in live and fixed cells. *Methods Cell Biol* **41**, 195-209.

Czirok, A., Rupp, P. A., Rongish, B. J. and Little, C. D. (2002). Multi-field 3D scanning light microscopy of early embryogenesis. *J Microsc* **206**, 209-217.

Drobizhev, M., Makarov, N. S., Tillo, S. E., Hughes, T. E. and Rebane, A. (2011). Two-photon absorption properties of fluorescent proteins. *Nat Methods* **8**, 393-399.

Drobizhev, M., Stoltzfus, C., Topol, I., Collins, J., Wicks, G., Mikhaylov, A., Barnett, L., Hughes, T. E. and Rebane, A. (2014). Multiphoton Photochemistry of Red Fluorescent Proteins in Solution and Live Cells. *The Journal of Physical Chemistry B* **118**, 9167-9179.

Eyal-Giladi, H. and Kochav, S. (1976). From cleavage to primitive streak formation: a complementary normal table and a new look at the first stage of the development of the chick. I. General morphology. *Dev. Biol.* **49**, 321-337.

Feng, G., Mellor, R. H., Bernstein, M., Keller-Peck, C., Nguyen, Q. T., Wallace, M., Nerbonne, J. M., Lichtman, J. W. and Sanes, J. R. (2000). Imaging neuronal subsets in transgenic mice expressing multiple spectral variants of GFP. *Neuron* **28**, 41-51.

Foudi, A., Hochedlinger, K., Van Buren, D., Schindler, J. W., Jaenisch, R., Carey, V. and Hock, H. (2009). Analysis of histone 2B-GFP retention reveals slowly cycling hematopoietic stem cells. *Nat Biotechnol* **27**, 84-90.

Hamburger, V. and Hamilton, H. L. (1951). A series of normal stages in the development of the chick embryo. *J Morph* **88**, 49-92.

Kanda, T., Sullivan, K. F. and Wahl, G. M. (1998). Histone-GFP fusion protein enables sensitive analysis of chromosome dynamics in living mammalian cells. *Curr Biol* **8**, 377-385.

Kawahara-Miki, R., Sano, S., Nunome, M., Shimmura, T., Kuwayama, T., Takahashi, S., Kawashima, T., Matsuda, Y., Yoshimura, T. and Kono, T. (2013). Next-generation sequencing reveals genomic features in the Japanese quail. *Genomics* **101**, 345–353.

Krull, C. (2004). A primer on using in ovo electroporation to analyze gene function. *Dev Dyn* **229**, 433-439.

Kulesa, P., Bronner-Fraser, M. and Fraser, S. (2000). In ovo time-lapse analysis after dorsal neural tube ablation shows rerouting of chick hindbrain neural crest. *Development* **127**, 2843-2852.

Development • Accepted manuscript

Kulesa, P. M. and Fraser, S. E. (1998). Neural crest cell dynamics revealed by time-lapse video microscopy of whole embryo chick explant cultures. *Dev Biol* **204**, 327-344.
Kulesa, P.M. and Fraser, S.E. (2011) Live imaging of avian embryos. Imaging in Developmental Biology: A Laboratory Manual. Cold Spring Harbor Press. 85-99.
Lansford, R., Bearman, G. and Fraser, S. E. (2001). Resolution of multiple green fluorescent protein color variants and dyes using two-photon microscopy and imaging spectroscopy. *J Biomed Opt* **6**, 311-318.
Le Douarin, N. (1973). A biological cell labeling technique and its use in expermental embryology. *Dev Biol* **30**, 217-222.
Le Douarin, N. and Barq, G. (1969). [Use of Japanese quail cells as "biological markers" in experimental embryology]. *C R Acad Sci Hebd Seances Acad Sci D* **269**, 1543-1546.
Le Douarin, N. and Kalcheim, C. (1999). *The Neural Crest* (2nd edn): Cambridge University Press.
McGrew, M. J., Sherman, A., Ellard, F. M., Lillico, S. G., Gilhooley, H. J., Kingsman, A. J., Mitrophanous, K. A. and Sang, H. (2004). Efficient production of germline transgenic chickens using lentiviral vectors. *EMBO Rep* **5**, 728-733.
McGrew, M.J., Sherman, A., Lillico, S,G., Ellard, F.M., Radcliffe, P.A., Gilhooley, H.J., Mitrophanous, K.A., Cambray, N., Wilson, V., and Sang, H. (2008). Localised axial progenitor cell populations in the avian tail bud are not commited to a posterior Hox identity. *Development* **135**, 2289-2299.
Momose, T., Tonegawa, A., Takeuchi, J., Ogawa, H., Umesono, K. and Yasuda, K. (1999). Efficient targeting of gene expression in chick embryos by microelectroporation. *Development, Growth & Differentiation* **41**, 335-344.
Motono, M., Yamada, Y., Hattori, Y., Nakagawa, R., Nishijima, K.-i. and Iijima, S. (2010). Production of transgenic chickens from purified primordial germ cells infected with a lentiviral vector. *Journal of Bioscience and Bioengineering* **109**, 315-321.
Nakamura, H., Katahira, T., Sato, T., Watanabe, Y. and Funahashi, J. (2004). Gain- and loss-of-function in chick embryos by electroporation. *Mech Dev* **121**, 1137-1143.
Nishibori, M., Hayashi, T., Tsudzuki, M., Yamamoto, Y. and Yasue, H. (2001). Complete sequence of the Japanese quail (Coturnix japonica) mitochondrial genome and its genetic relationship with related species. *Animal Genetics* **32**, 380-385.
Noden, D. M. and Trainor, P. A. (2005). Relations and interactions between cranial mesoderm and neural crest populations. *Journal of Anatomy* **207**, 575-601.
Poynter, G., Huss, D. and Lansford, R. (2009). Japanese quail: an efficient animal model for the production of transgenic avians. *Cold Spring Harb Protoc* **2009**, pdb emo112.
Ridenour, D. A., McKinney, M. C., Bailey, C. M. and Kulesa, P. M. (2012). CycleTrak: a novel system for the semi-automated analysis of cell cycle dynamics. *Dev Biol* **365**, 189-195.
Rozbicki, E., Chuai, M., Karjalainen, A. I., Song, F., Sang, H. M., Martin, R., Knolker, H. J., MacDonald, M. P. and Weijer, C. J. (2015). Myosin-II-mediated cell shape changes and cell intercalation contribute to primitive streak formation. *Nat Cell Biol* **17**, 397-408.
Sakaue-Sawano, A., Kurokawa, H., Morimura, T., Hanyu, A., Hama, H., Osawa, H., Kashiwagi, S., Fukami, K., Miyata, T., Miyoshi, H., et al. (2008). Visualizing spatiotemporal dynamics of multicellular cell-cycle progression. *Cell* **132**, 487-498.
Salic, A. and Mitchison, T. J. (2008). A chemical method for fast and sensitive detection of DNA synthesis in vivo. *Proceedings of the National Academy of Sciences* **105**, 2415-2420.
Sambrook, J. and Russell, D. W. (2001). *Molecular Cloning: A Laboratory Manual* (3rd edn). Cold Spring Harbor, NY: Cold Spring Harbor Laboratory Press.
Sato, Y. and Lansford, R. (2013). Transgenesis and imaging in birds, and available transgenic reporter lines. *Development Growth & Differentiation* **55**, 406-421.
Sato, Y., Poynter, G., Huss, D., Filla, M. B., Czirok, A., Choi, J. M., Rongish, B. J., Little, C. D., Fraser, S. E. and Lansford, R. (2010). Dynamic analysis of vascular morphogenesis using transgenic quail embryos. *PLoS ONE* **5**, e12674.
Scott, B. B. and Lois, C. (2005). Generation of tissue-specific transgenic birds with lentiviral vectors. *Proc Natl Acad Sci U S A* **102**, 16443-16447.

Seidl, A. H., Sanchez, J. T., Schecterson, L., Tabor, K. M., Wang, Y., Kashima, D. T., Poynter, G., Huss, D., Fraser, S. E., Lansford, R., et al. (2013). Transgenic quail as a model for research in the avian nervous system: a comparative study of the auditory brainstem. *J Comp Neurol* **521**, 5-23.

Stern, C. D. (2005). The Chick: A great model system becomes even greater. *Developmental Cell* **8**, 9-17.

Tschopp, P., Sherratt, E., Sanger, T. J., Groner, A. C., Aspiras, A. C., Hu, J. K., Pourquie, O., Gros, J. and Tabin, C. J. (2014). A relative shift in cloacal location repositions external genitalia in amniote evolution. *Nature* **516**, 391-394.

Tumbar, T., Guasch, G., Greco, V., Blanpain, C., Lowry, W. E., Rendl, M. and Fuchs, E. (2004). Defining the epithelial stem cell niche in skin. *Science* **303**, 359-363.

Vadakkan, T. J., Culver, J. C., Gao, L., Anhut, T. and Dickinson, M. E. (2009). Peak Multiphoton Excitation of mCherry Using an Optical Parametric Oscillator (OPO). *Journal of fluorescence* **19**, 1103-1109.

Voiculescu, O., Papanayotou, C. and Stern, C. D. (2008). Spatially and temporally controlled electroporation of early chick embryos. *Nat Protoc* **3**, 419-426.

Weake, V. M. and Workman, J. L. (2008) Histone Ubiquitination: Triggering Gene Activity. *Molecular Cell* **29**, 653-663.

Zeng, G., Taylor, S. M., McColm, J. R., Kappas, N. C., Kearney, J. B., Williams, L. H., Hartnett, M. E. and Bautch, V. L. (2007). Orientation of endothelial cell division is regulated by VEGF signaling during blood vessel formation. *Blood* **109**, 1345-1352.

Development ● Accepted manuscript

Supplementary methods

Southern blot analysis for the *chFP* transgene

Genomic DNA (5 µg/lane) was electrophoresed in a 0.8% agarose/Tris acetate (TAE) gel at 46 V for 5 h. Gels were then denatured for 30 min at room temperature in 0.5 M NaOH, 1.5 M NaCl, neutralized for 30 min in 0.5 M Tris-HCl (pH 7.0), rinsed for 30 min in 20× SSC then transferred to a nylon membrane (Hybond, Amersham) overnight at room temperature. The blot was rinsed in 2× SSC, allowed to dry on 3 mm filter paper, cross-linked (Stratagene) and stored dry between sheets of 3 mm filter paper until used. A 646 bp probe against the Woodchuck hepatitis virus promoter response element (WPRE) region of the transgene was generated by cutting the pLenti.PGK1:eGFP lentivector with *Bgl*II and *Sal*I, gel isolating the linearized fragment, and labeling it with ^{32}P dCTP (Perkin Elmer) using a random priming kit (RediPrime II, Amersham, GE Healthcare), and hybridized. Blots were imaged using a Storm 840 phosphorimager (Molecular Dynamics).

Cell proliferation assay

The Click-iT EdU assay (Invitrogen) was used to assay *in vivo* cell proliferation according to manufacturers recommendations. The EdU assay uses a copper catalyzed cycloaddition reaction between the terminal alkyne group of the thymine analog EdU (5'-ethynyl-2'-deoxyuridine) and a fluorophore-conjugated azide molecule. The EdU assay (Warren et al., 2009) was carried out on cultured quail embryo. EdU (Click-iT EdU kit, Cat. #C10083 Invitrogen) was diluted in PBS at 10 mM (stock solution). 50 µl of working dilution (500 µM) was dropped on embryos incubated for 40 h (developmental stages 7-10), which were incubated for 6 h. The embryos were washed with PBS and fixed in 4% formaldehyde [36% formaldehyde (47608, Sigma) diluted to 4% in PBS]. The percentage of EdU-positive cells and level of chFP signals were quantified using the spot function of Imaris (Bitplane) software. Between 72 and 643 cells were analyzed for each embryonic territory. The linear correlation is significant at a level of 0.05. The standard error of the slope was found from the sum of squared differences of x and y for the five data points and used to calculate a t statistic of –3.36. For a two-tailed test, this t statistic correlates to a P-value of 0.044 at three degrees of freedom. Standard error of the mean was computed and is represented as error bars.

Microscopy

For static whole-mount images, the embryos were isolated from the yolk using paper rings, washed in PBS, fixed in 4% paraformaldehyde/PBS at 4ºC for 16 hours, washed again in PBS, and stained with DAPI (0.5 µg/µl) for 2 h at room temperature. Embryos were then washed in PBS and mounted between two #1 coverslips using Permafluor mounting media (Thermo Scientific) and stored in the dark at 4ºC until imaging. For vibratome sectioning, the chFP$^+$ DAPI-stained embryos were embedded in a warm mixture of 3% agarose and acrylamide/bis-acrylamide/TEMED (Germroth et al., 1995). Cross-linking was initiated by the addition of 0.1% ammonium persulfate while on ice. The resulting blocks were serially cross-sectioned at 70 µm on a Leica 1200 vibratome. For dynamic images, embryos were isolated from the yolk using a modified paper ring EC (Early Chick) culture system (Chapman et al., 2001). Briefly, a thin bed of agar/albumin was poured into several 35 mm culture dishes and a single two-well Lab Tek chambered #1 coverglass slide (Thermo Scientific) and allowed to solidify. After removal from the yolk, the embryos were briefly washed in sterile PBS and placed dorsal side down on the agar/albumin bed in the 35 mm Petri dishes. The embryos were returned to the 37ºC incubator for 2 h to recover then screened under an Olympus MVX10 stereomicroscope for the presence of the fluorescent reporter and normal morphology. Selected embryos were transferred dorsal side down onto the agar bed of the two chamber imaging slide and the lid was sealed with parafilm. The slide was mounted onto the stage of the confocal microscope which had been pre-warmed to 37ºC using an electronically controlled environmental chamber (Pecon). The embryo was incubated on the microscope for 2 h to allow the embryo to settle down into the agar/albumin layer before imaging was initiated.

3D imaging metadata for various developmental stages
Microscope metadata: Zeiss LSM 780 (inverted) equipped with 34 channel GaAsp Spectral Detectors, 5 laser lines (405, 458, 488, 514, 561 and 633 nm), and run with ZEN 2011 system software was used to collect all the 3D images of various developmental stages.
Microscope metadata: Zeiss LSM 780 inverted confocal microscope; Plan-Apochromat 20x/0.8 WD=0.55 M27 objective; Ex 405 (1.2%)/Em 409-584; Ex 561 (5.0%)/Em 571-695; Pixel dwell time, 12.6 µsec; mean of 2 line scans.

Additional metadata for each collection is detailed below:

Developmental stage X (Fig. 1B,C)
Dimensions: 5020.62 x 5062.96 x 35.00 μm^3 (16 *z*-sections); Resolution: 1.20 pixels per µm; Voxel size: 0.83 x 0.83 x 2.5 μm^3; Bits per pixel: 16.

Developmental stage 11 (Fig. 1D,E)
Dimensions: 1208.04 x 5426.62 x 244.0 μm^3 (61 *z*-sections); Resolution: 1.20 pixels per µm; Voxel size: 0.83 x 0.83 x 4 μm^3; Bits per pixel: 16.

3D imaging by two-photon microscopy (Fig. S6)
A fixed stage 10 Tg(PGK1:H2B-chFP) embryo was mounted in glycerol.
Microscope metadata: Zeiss LSM 780 inverted confocal microscope powered by a Titanium:Sapphire (Ti:Sa) laser (810 nm pump) coupled to an OPO system (Coherent); C-Achroplan 32x/0.85 W Corr M27 objective (Zeiss); Ex 1050 (50%); main beam splitter MBS 690+ was used as well as BS-MP-760. zoom was set up at 0.6; pixel dwell time, 25.2 µsec; mean of 2 line scans; master gain was set up at 812. The NDD external detector BIG (Zeiss) was used to collect the signal.

4D imaging metadata for various time-lapse experiments
For dynamic imaging we used whole-mount *ex ovo* avian embryo culture previously described (Drake et al., 1992; New, 1955; Sato et al., 2010). A Zeiss LSM 510 META inverted confocal microscope equipped with an onstage incubator maintained the temperature at 36ºC during imaging was used to acquire Movies 1-2 and 4-10.

Multicolor mosaic stitching
Mosaic stitching was performed using Zeiss Zen, or Fiji after color-balance correction. *xy* translation between images was evaluated using single *z*-slices, or maximum-intensity projections when possible.

Image analysis
Image analysis was performed using ImageJ (US National Institutes of Health), Fiji (http://fiji.sc/), MATLAB (MathWorks) and Imaris (Bitplane). Since all cells in the Tg(PGK1:H2B-chFP) quail contain a detectable fluorescent label, the number of cells to be followed is large (hundreds to thousands), requiring 'multiple-particle tracking.' Cell behaviors were analyzed using Imaris (Bitplane), Fiji and MATLAB software. LSM formatted images classified into image sets were processed using various image analysis tools/algorithms. The data output from the image analysis pipeline is a set of cell parameters and images for visual inspection. Information from tracked cells was extracted from processed image sets for further data analysis. Typical parameters obtained from each image set include nuclear perimeter, volume and mean pixel intensity. Other measurements first require the identification of individual cells across multiple frames in order to determine parameters of cell motility (e.g. velocity, direction, persistence), rates and orientations of cell division, and daughter cell and tissue-specific cell movements. The data extracted from image sets are saved as a set of Excel files for statistical analysis.

All images were stored in the original .lsm format and copies were manipulated using Photoshop CC (Adobe) and movies were annotated in Premiere Pro CC (Adobe). All original high-resolution image sets are available upon request.

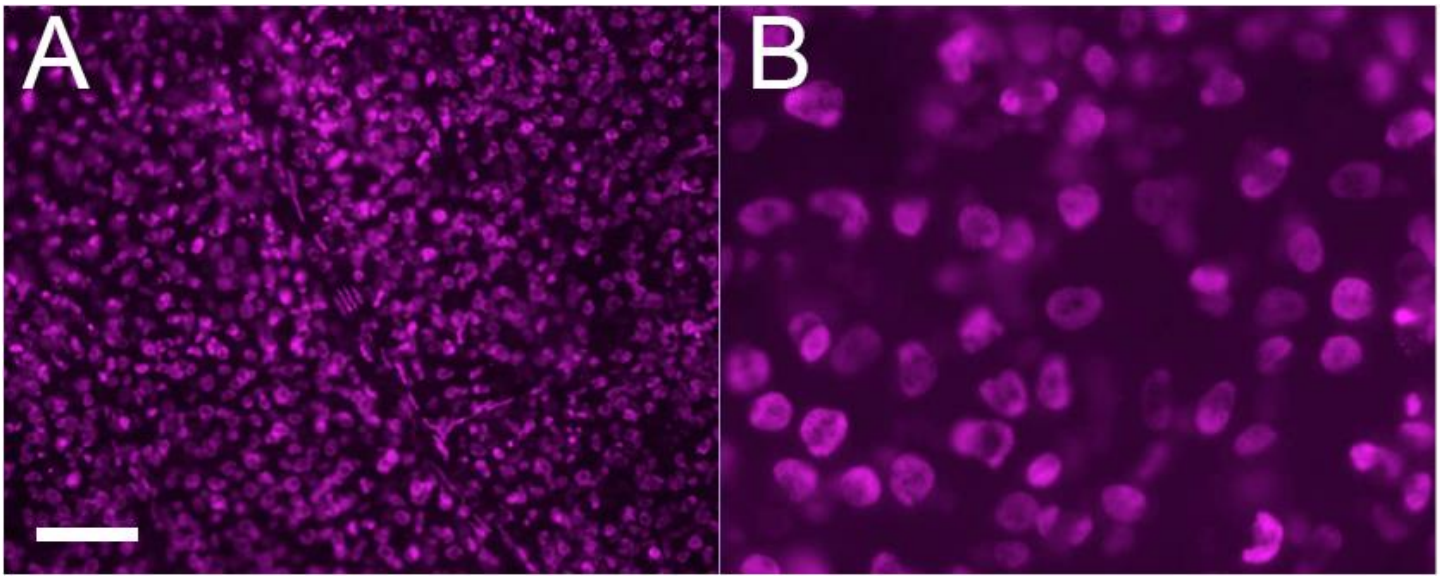

Fig.S1. Fluorescent stereomicroscope image of the CAM inside a newly hatched Tg(PGK1:H2B-chFP) egg. (A) Fluorescence dissecting microscope acquired image of H2B-chFP+ calls that comprise the CAM within the shell from the offspring of a Tg(PGK1:H2B-chFP) founder quail. (B) Same CAM as in (A) at 5X higher magnification showing cell nuclei expressing H2B-chFP. Scale bar, 20 um for A and 100 um for B.

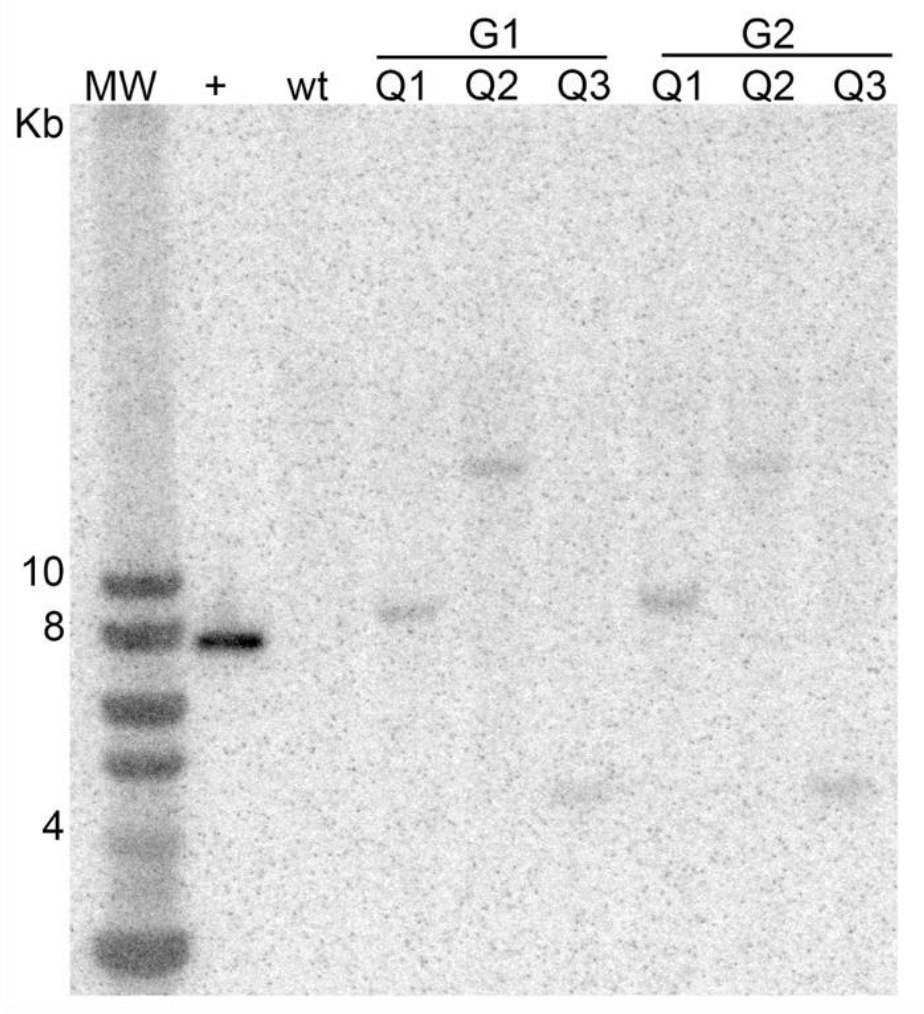

Fig.S2. Screening hatchling genomic DNA by Southern blot analysis.

Southern blot analysis of genomic DNA isolated from the chorioallantoic membrane of the eggshell from 3 different chimeric founders (G0). The gDNA was digested with Spe1, which cuts once inside the transgene, separated by gel electrophoresis and transferred to a nylon membrane. The blot was hybridized with a 646bp 32P-labeled probe designed to hybridize with the WPRE element within the transgene (Fig.1A). Three transgenic lines with single transgene integrations at distinct locations were identified and labeled as Q1 (9kb), Q2 (>10kb) and Q3 (5kb). When bred to a WT, these first generation (G1) birds produced genotypically positive second generation (G2) hatchlings as expected. + lane is the pPGK1:H2B-chFP lentivector shown in Fig.1A. WT lane is gDNA from a non-transgenic hatchling. MW lane is molecular weight markers in kilobases.

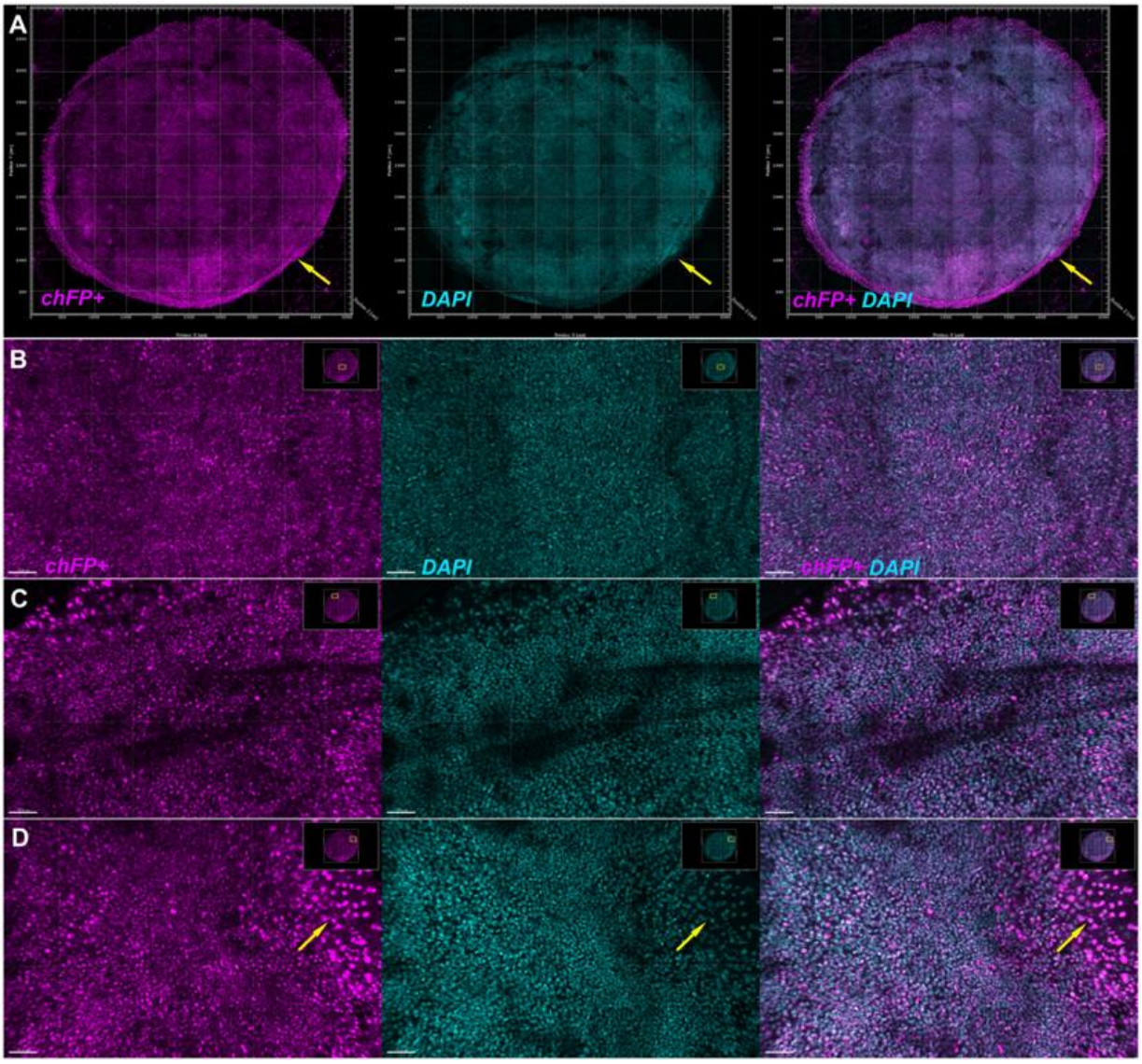

Fig.S3. Ubiquitous expression of PGK1:H2B-chFP transgene in developmental stage 2 embryos.

(A) Confocal microscope acquired images for chFP$^+$, DAPI, and chFP$^+$/DAPI overlay of a developmental stage 2 Tg(PGK1:H2B-chFP) quail embryo. Tg(PGK1:H2B-chFP) embryos ubiquitously express H2B-chFP during developmental stage 2. Note that the DAPI and chFP$^+$ relative fluorescence intensities do not always correlate, which is best discerned in the chFP$^+$/DAPI overlays. Putative hypoblast cells located at the posterior end of the embryo (A) and extra embryonic germ wall cells consistently display very high levels of chFP fluorescence (marked by yellow arrows in A, D). The relative chFP fluorescence intensity of these cells is 4-8-fold higher than the vast majority of the embryonic and extra embryonic cells (data not shown). (B-D) higher magnification images to confirm ubiquitous and heterogenous chFP+ expression. The precise location of the magnified images in terms of the entire stage 2 embryo can be seen in the upper right corner of each image. Dorsal view; anterior at top for all images. A) Grid scale marked every 500 um along xy axes; B-D) Lower left scale bar: 70 um. Dimensions: 5232.06 x 5244.51 x 92.0 μm^3 (23 *z*-sections); Resolution: 0.72 pixels per μm; Voxel size: 1.38 x 1.38 x 4 μm^3; Bits per pixel: 16.

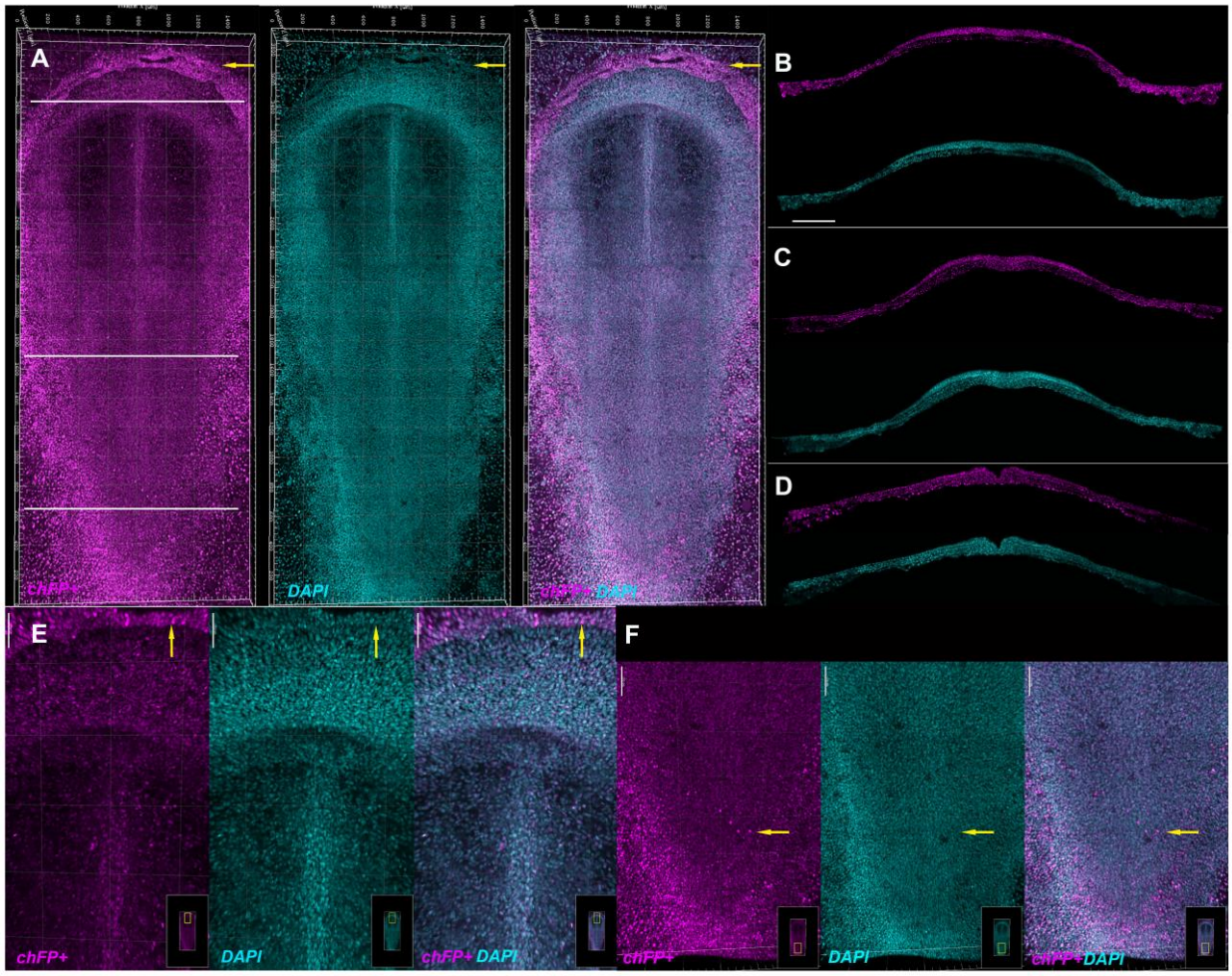

Fig.S4. Ubiquitous expression of PGK1:H2B-chFP transgene in developmental stage 5 embryos.

(A) Confocal microscope acquired images for chFP$^+$, DAPI, and chFP$^+$/DAPI overlay of a developmental stage 5 Tg(PGK1:H2B-chFP) quail embryo and (E-F) higher magnification images to confirm ubiquitous and heterogenous chFP$^+$ expression. Note that the DAPI and chFP$^+$ relative fluorescence intensities do not always correlate, which is best discerned in the chFP$^+$/DAPI overlays. Some extra embryonic (A, E, and F) and embryonic (A and F) cells display very high levels of chFP fluorescence (marked by yellow arrows). (B-D) Embryos were vibratome sectioned to generate transverse sections at approximately the A-P region noted by the white lines in A and imaged by confocal microscopy to confirm ubiquitous and heterogenous chFP$^+$ expression. Dorsal view; anterior at top for all images. A) Grid scale marked every 200 um along *xy* axes; B-D) scale bar: 200um; E-F) Vertical upper left scale bar: 100 um.

Dimensions: 1584.98 x 3860.74 x 148 µm^3 (37 *z*-sections); Resolution: 1.20 pixels per µm; Voxel size: 0.83 x 0.83 x 4 µm^3; Bits per pixel: 16.

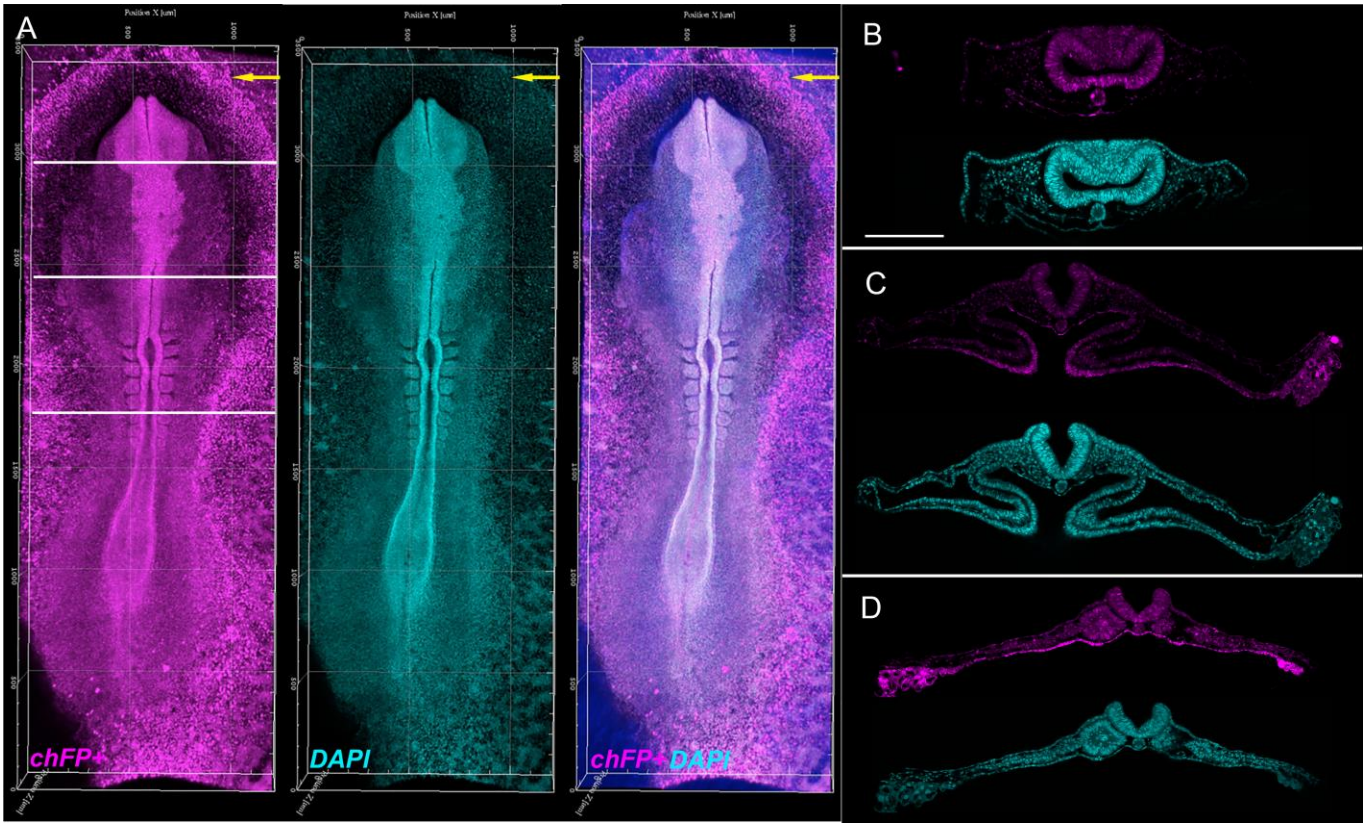

Fig.S5. Ubiquitous expression of PGK1:H2B-chFP transgene in developmental stage 9 embryos.

(A) Confocal microscope acquired images for chFP^{+}, DAPI, and chFP^{+}/DAPI overlay of a developmental stage 9 Tg(PGK1:H2B-chFP) quail embryo. (B-D) Embryos were vibratome sectioned to generate transverse sections at approximately the A-P region noted by the white lines in A and imaged by confocal microscopy to confirm ubiquitous and heterogeneous chFP^{+} expression. Dorsal view; anterior at top for all images. Dorsal view; anterior at top for all images. A) Grid scale marked every 500 um along xy axes. B-D) scale bar: 200um. Dimensions: 1210.53 x 3500.40 x 152 µm^3 (38 *z*-sections); Resolution: 1.20 pixels per µm; Voxel size: 0.83 x 0.83 x 4 µm^3; Bits per pixel: 16.

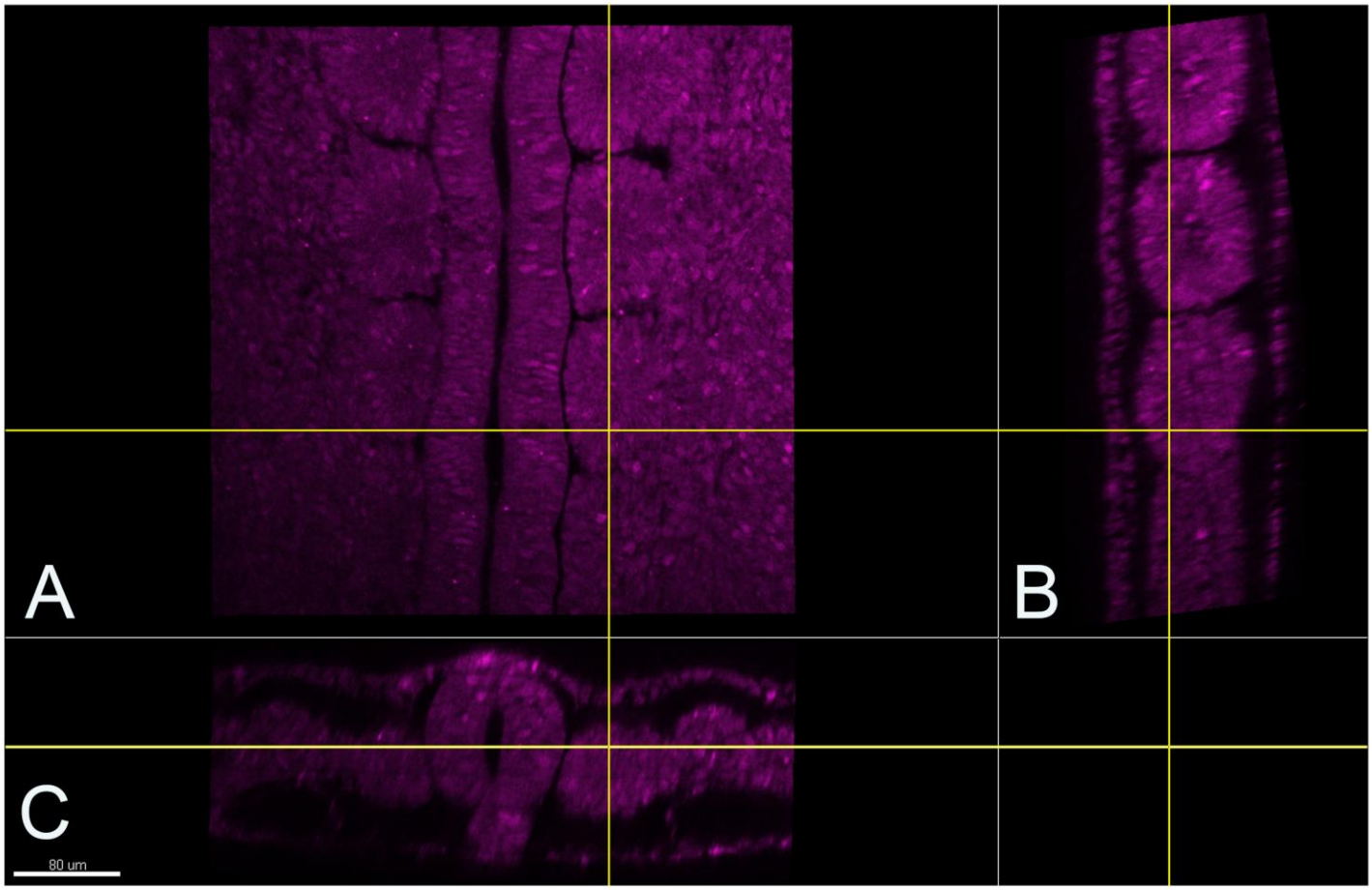

Fig. S6. 3D reconstruction of PGK1:H2B-chFP signal visualized by two-photon confocal microscopy.

3D reconstruction of PGK1:H2B-chFP signal in the trunk of a fixed stage 10 embryo visualized by 2 photon microscopy.(A) XY plane, (B) YZ plane, (C) XZ plane. Note that fluorescent signal can be detected throughout the embryo. Anterior is at the top in A and B. Dorsal is on the left in B. Ventral is on the bottom in C. Yellow lines demarcate the level at which planes are seen in neighboring panel. Image has been cropped using the crop 3D function of Imaris to remove regions without signal above and below the embryo. Scale bar for A-C is 80um.

Dimensions: 442 x 442 x 191 μm^3 (191 z-sections); Resolution: 0.865 pixels per µm; Voxel size: 0.865 x 0.865x 1 μm^3; Bits per pixel: 16.

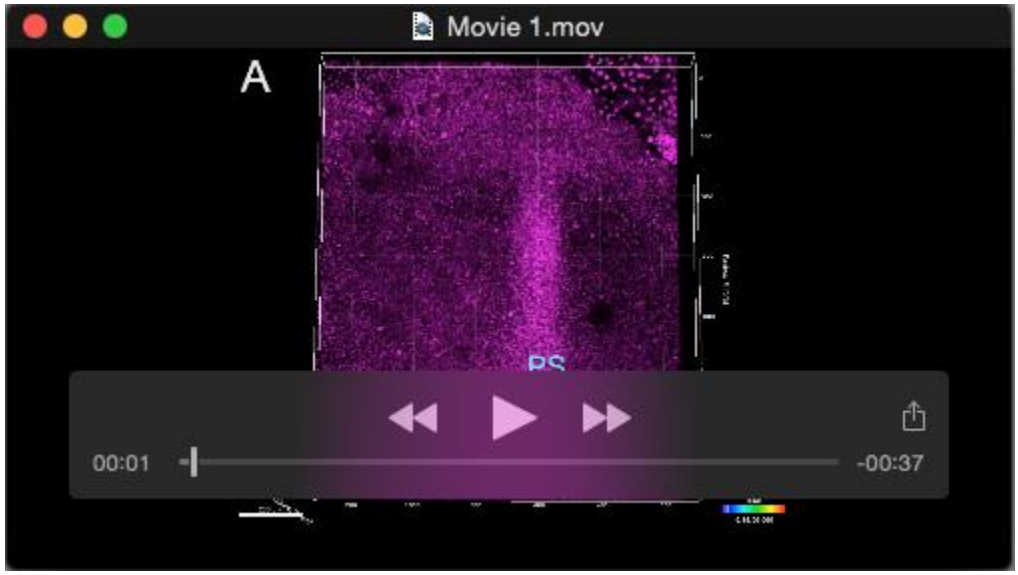

Movie 1. 4D imaging of gastrulating Tg(PGK1:H2B-chFP) embryo. 4D rendering of embryonic cells labeled with nuclear localized chFP and imaged by time-lapse confocal fluorescence microscopy over 86 time points at 15-min intervals for a total of 21:30 hrs. The embryo is oriented with the anterior end (A) on the left in order to view with higher resolution on a computer screen. The gastrulating embryo elongates along the A-P axis as converging epiblast cells intercalate along the midline to form the PS (~3:00:00 time point). The head fold process begins (~5:30:00) concomitant with continued A-P elongation. Somites 1 begin to form bilateral and adjacent to the PS (~8:30:00) and continue until the movie ends at the 8-somite stage (21:30:00). A-P elongation along the midline appears centered anterior to the future sites of somite 1 formation. Some extra embryonic within the area opaque consistently display very high levels of chFP fluorescence.

Ventral view. Lower left scale bar: 200 um; grid scale marked every 500 um along xy axes; time scale in lower right corner; A, anterior; D, dorsal; L, lateral; AO, area opaque; PS, primitive streak; HF, head fold. Lower right 3D arrows indicate that the embryo is oriented with anterior (A) to the left, lateral (L) to the bottom, and ventral (V) into the page.

Microscope metadata: Zeiss 510 META inverted, 20X/0.8 NA Plan-Apochromat; Ex 561 (15%)/Em LP 575.

Dimensions: 2812.51 x 1687.5 x 162 μm^3; Voxel size 2.2 x 2.2 x 6.0 μm^3.

Acquisition time: Image montage (5 x 3 x 22) at 15 min intervals per *xyz* tile for 86 time points (*t*) or 21:30:00 hrs was made by stitching *xyz* image sets across *t* with AIM LSM4.0 software.

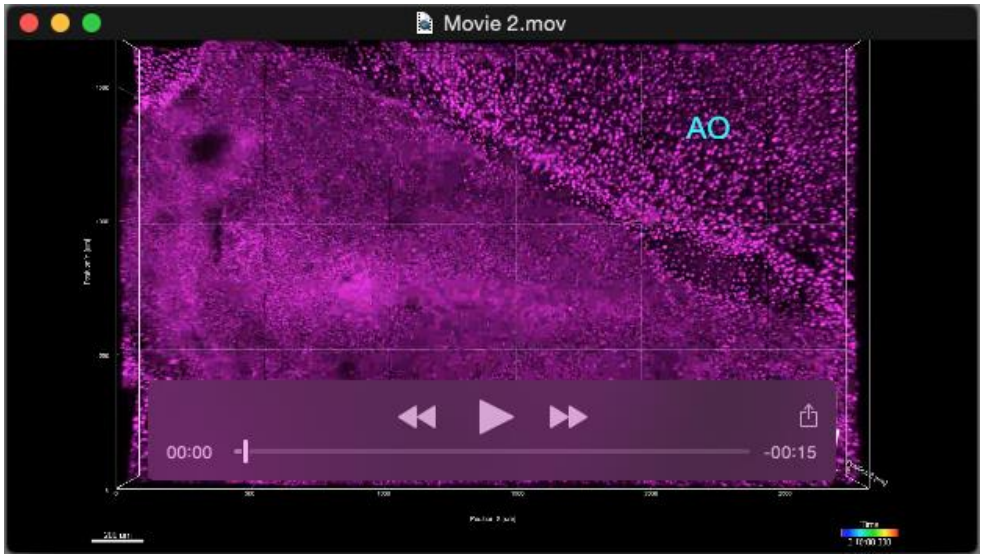

Movie 2. Cell and tissue movements during head fold process.

Compare with Movie 1 and Fig.3. Movie 2 derives from Movie 1, but was rotated 90 around the vertical axis and 180 around the horizontal axis for a preferred viewing perspective; the image set was also cropped initially in the *xy* dimensions and later in the *z* dimension in order to direct the attention of the reader and to reduce computational time. The embryo is oriented with the anterior end on the top.

(A) Maximum intensity projection of head fold process showing elongation along the A-P axis as converging epiblast cells intercalate along the midline thrusting the PS and adjacent tissue anterior until they fold ventrally and then descends in the posterior direction. As the ventral tissue moves posterior, adjacent lateral tissue simultaneously folds toward the midline to form the AIP.

(B) Tracking cells to show direction and speed of migration. The cell tracks are shown as white 'dragon tails' that represent a cell's location for the previous four time points (60 minutes) are overlayed on Movie 2A.

(C) The cell tracks are color coded 'dragon tails' that represent a cell's location and movement along the *y*-axis (-50 Anterior to 50 Posterior) for the previous four time points (60 minutes) are overlayed on Movie 2A.

(D) Tracking cells to indicate movement along the *y*-axis, direction, and speed of migration. The cell tracks are color-coded 'dragon tails' that represent a cell's location and movement along the *y*-axis (-50 Anterior to 50 Posterior) for the previous four time points (60 minutes).

(E) Movie 2A is re-oriented to better visualize the *z*-movements of cells and tissue. The anterior end is oriented into the screen and the central axis is tipped slightly to the right. This gives the viewer a perspective of looking into the forming AIP and permits the medio-lateral tissue movements to better visualized in 3D over time.

Ventral view. Lower left scale bar: 200 um; grid scale marked every 500 um along xy axes; time scale in lower right corner; Ant, anterior; AO, area opaque; PS, primitive streak; HF, head fold. Skewed perspective is 130% zoom. Lower left 3D arrows indicate that the embryo is oriented with anterior (A) to the top, lateral (L) to the left, and dorsal (D) into the page.

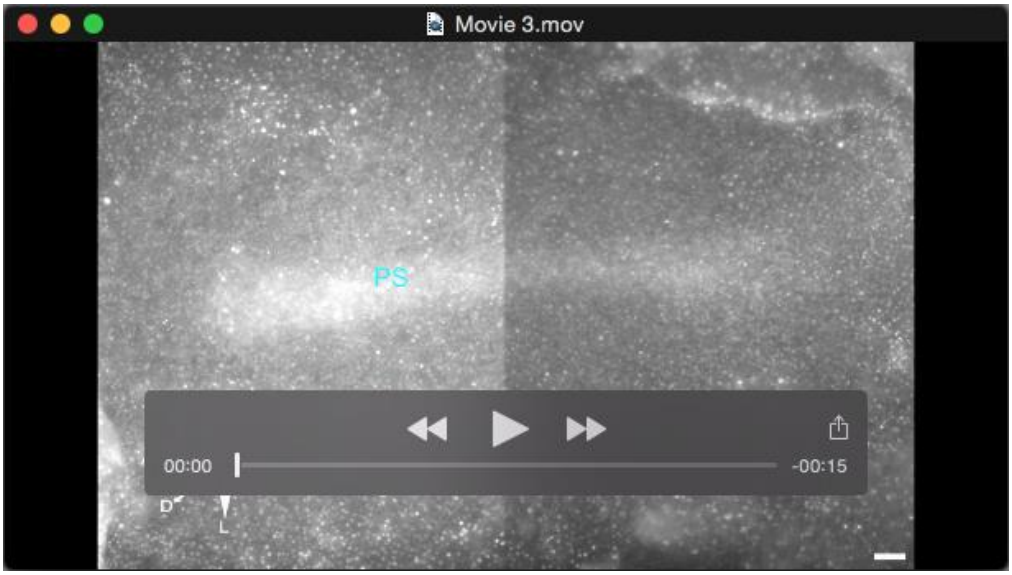

Movie 3. Wide-field fluorescence microscopy to evaluate large-scale tissue displacements.

Wide-field fluorescence microscopy of living Tg(PGK1:H2B-chFP) embryos captures the collective biological motion patterns that characterize early embryogenesis, including gastrulation, neurulation, somitogenesis, cardiogenesis, and neurogenesis recorded across 4 orders of spatial (400nm to 4 mm) and (1 minute to 1000 min) temporal resolution. The time-lapse sequence of Tg(PGK1:H2B-chFP) quail development begins during gastrulation and shows the movement of thousands of cells with the upper epiblast cells converging en masse toward the PS at the midline and cells of the bottom hypoblast layer moving radially outward and anterior (Frames 1-60). The PS extends anteriorly along the midline to orient the embryo along the A-P and D-V axes (Frames 1-75). As gastrulation proceeds, the A-P extension reaches a temporary maximum as the anterior head region folds back on itself, extends and moves posteriorly (Frame 75), A-P elongation continues and somites begin to form (Frame 83). As the head fold curves at the anterior end of the embryo, the tail folds at the posterior end, and then the lateral body folds at the sides of the embryo transforming the relatively flat gastrula into a three-dimensional organism. As AIP regression proceeds, the heart fields soon converge at the midline atop the regressing AIP, and assemble into the linear heart (H) tube by the end of the movie (Frame 140).

Ventral view. Scale bar in lower right corner represents 100 um; elapsed time and frame number are noted across the top of the movie; PS, primitive streak; HF, head fold; N, notochord; S, somite; AIP, anterior intestinal portal; Magenta asterisk (*) denotes approximate location of the regressing Hensen's node. Skewed perspective is 130% zoom. Lower left 3D arrows indicate that the embryo is oriented with anterior (A) to the left, lateral (L) to the bottom, and dorsal (D) into the page.

Microscope metadata: Brightfield and epifluorescence acquired on a Leica DM6000B upright microscope with the ventral side of the embryo facing the objective using a 5X/0.12P PL Fluotar objective, epifluroescence captured through Chroma mCherry/Texas Red filter set ET560/40ex ET630/75em with a T585lp beam splitter detected using a Retiga SRV deep cooled CCD camera. For each field and optical mode, images were acquired in 5 focal planes, so that the embryo remains in focus during extended recording times. The acquired images were processed to make full-scale images registered to correct for *xy* shifts during the experiment. (Czirok et al., 2002). The time-lapse movie was trimmed to 140 time points (20:40:35 hrs) in order to end at developmental stage 11.

Dimensions: 1796 x 2544 um^2; Pixel size 1.29 um^2 and the extended depth of field processed image encompassing 310 □m z resolution acquired and processed using KU TiLa acquisition and ImageJ for post processed image stack manipulations.

Acquisition time: Image montage (1 x 2 x 5) at ~10 min intervals per *xyz* tile as indicated by time stamps recorded at the initiation of each montage acquisition. Brightfield exposure times of 0.015 seconds and epifluroescent exposure times of 1.5 seconds were used.

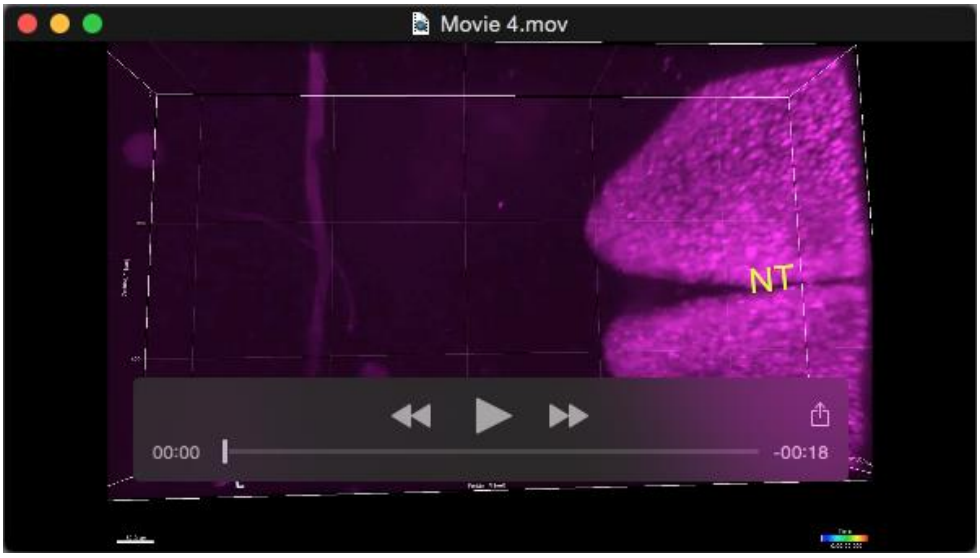

Movie 4. 4D imaging of cell movements during head formation using Tg(PGK1:H2B-chFP) embryo.

4D rendering of forming head region of Tg(PGK1:H2B-chFP) embryo over 107 time points at 5:10-min intervals. The anterior neuropore closes as NNE cells collectively move in anterior and ventral direction until frame 17, when the anterior edge of the embryo is at the 800 um X grid. The embryo elongates to the left as the NT elongates until frame 40, when the anterior edge of the embryo is at the 400 um X grid. As the anterior movement subsides, NC cells begin to delaminate from the NT and migrate bilaterally and ventrally along the inner side of the non-neural ectoderm (marked by cyan arrows).

Dorsal view. Lower left scale bar: 200 um; grid scale marked every 200 um along xy axes; time scale in lower right corner; A, anterior; NT, neural tube; NC, neural crest. Lower left 3D arrows indicate that the embryo is oriented with anterior (A) to the left, lateral (L) to the bottom, and ventral (V) into the page.

Microscope metadata: Zeiss 510 META inverted; 20X/0.8 NA Plan-Apochromat; Ex 561 (15%)/Em LP 575.

Dimensions: 1125.0 x 562.5 x 228 μm^3; Voxel size: 1.1 x 1.1 x 6.0 μm^3.

Acquisition time: Image montage (2 x 1 x 38) at 5:10 min intervals per *xyz* for a total of 10 hours, was made by stitching *xyz* image sets across *t* with AIM LSM4.0 software.

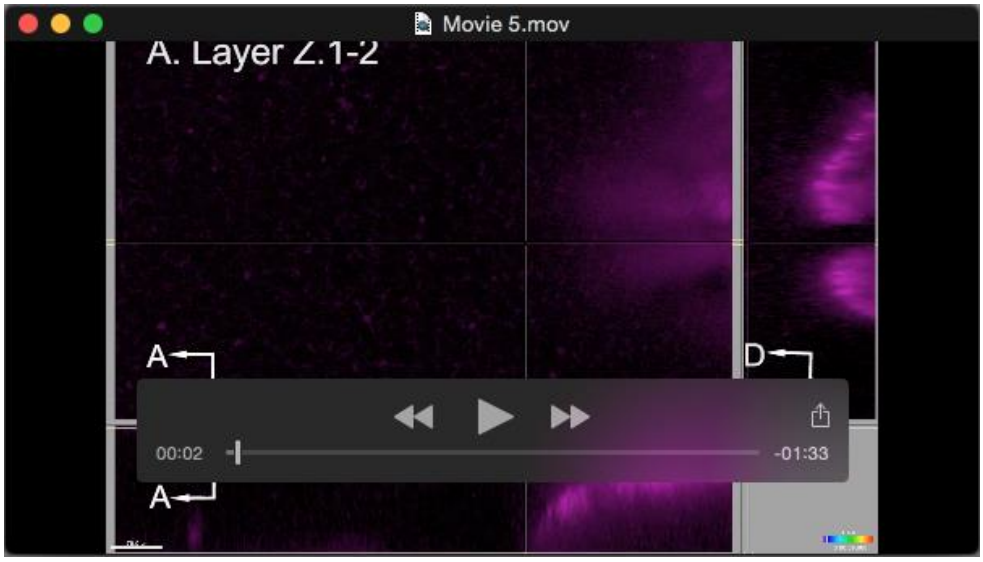

Movie 5. 4D imaging of distinct cell behaviors in different z layers during head formation.

Movie 5 derives from Movie 4; the image set has been cropped initially in the *xy* dimensions and later in the *z* dimension in order to direct the attention of the reader and to reduce computational time.

(A) Initial Z.1 movie segment focuses on proliferating non-neural ectoderm (NNE) are obvious throughout the z1 layer movie and are highlighted by a cyan circle.

(B) The Z.1 movie segment then transitions into a higher magnification view.

(C) Z.3-7 movie segment shows z3-7 layers and focuses on NC cells delaminating (denoted by cyan arrows) from the NT and migrating ventrolaterally beneath and along the NNE.

(D) Z.3-7 movie segment transitions into a higher magnification view.

(E) The Z.14 movie segment focuses on the NT as it moves anterior and presses against the anterior most NNE cells. The anterior end of the NT then flattens and bifurcates laterally as highlighted by black arrows. The head mesenchyme (M) is also apparent. The Z.14 movie segment then repeats without arrows (The Z.14 movie segment was fluorescently enhanced using Imaris and color inverted to view the deeper and thus dimmer cells.)

Dorsal view. Lower left scale bar: 200 um; grid scale marked every 200 um along xy axes; time scale in lower right corner; A, anterior; NT, neural tube; NC, neural crest. Arrows indicate how the various slices are oriented for anterior (A), lateral (L), and dorsal (D) directions. Microscope metadata same as Movie 4.

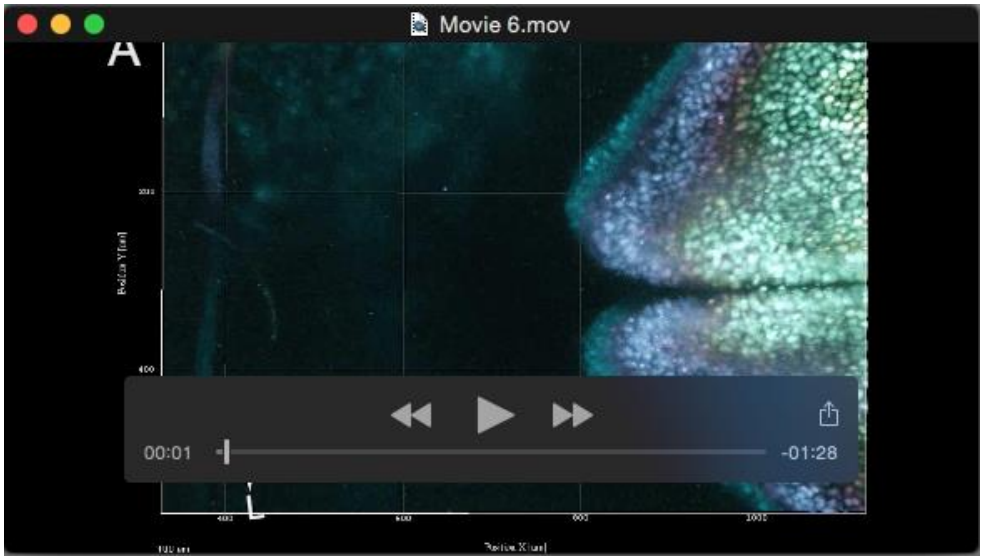

Movie 6. Color-coding of z layers helps visualize relative cell movements during head formation.

(A) To better visualize the relative movements chFP+ cells of cells and tissues in distinct z layers, we have color coded the image set with z1-2 in yellow, z3-7 in cyan, and z10-14 in magenta. Due to the curved structure of the dorsal head region, some NC cells are pseudo colored yellow and some ectoderm cells are pseudo colored cyan.

(B) NC cell egression (marked by cyan arrows) from the NT and bilateral migration are readily apparent with the ventral NT seen as a backdrop.

(C) Tracked cells are marked by an orange 'dragon tail' help visualize the speed and direction of individual cell movements overlay cells in Movie 6B.

(D) Tracked cells are marked by an orange 'dragon tail' help visualize the speed and direction of individual cell movements overlay cells in Movie 6A.

(E) 300% zoom of Movie 6D with focus on NC migration. Black circles surround putative yellow ectoderm cells to highlight the differences on cell movements within the distinct z layers. Cyan colored NC cells can be seen migrating beneath yellow ectoderm cells.

Dorsal view. Lower left scale bar: 200 um; grid scale marked every 200 um along xy axes; time scale in lower right corner; A, anterior; NT, neural tube; NC, neural crest. Lower left arrows indicate embryo is oriented for anterior (A) and lateral (L) directions.

Microscope metadata: Zeiss 510 META inverted, 20X/0.8 NA Plan-Apochromat; Ex 488 nm (12%)/Em BP 505-550; Ex 561 (15%)/Em LP 575.

Dimensions: 562.5 x 562.5 x 126 (21 z sections) μm^3; Voxel size: 2.2 x 2.2 x 6.0 μm^3; Bits per pixel: 8.

Acquisition time: Image montage (3 x 2 x 21), at 7:30 min intervals per *xyz* for a total of 29.5 hours was made by stitching *xyz* image sets across *t* with AIM LSM4.0 software.

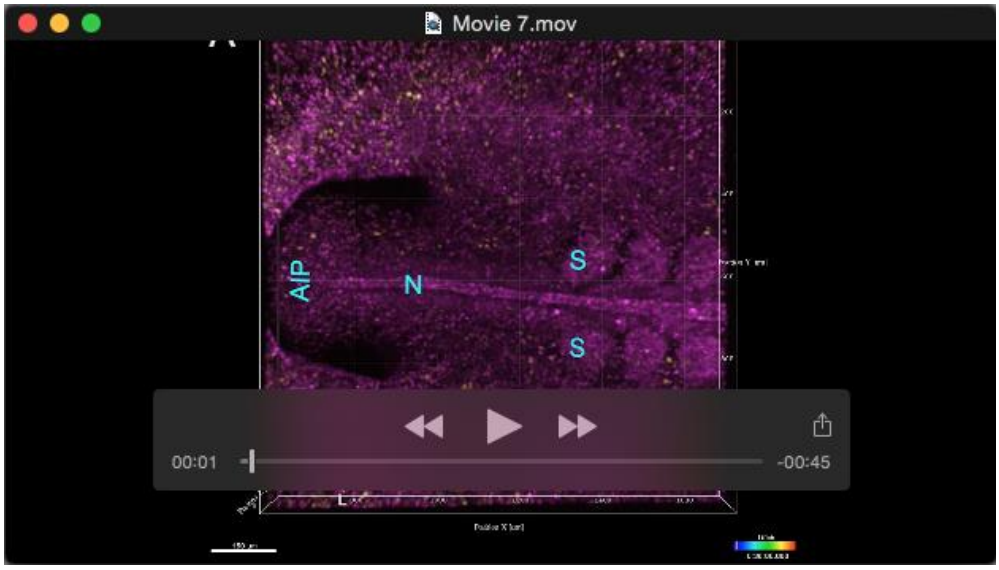

Movie 7. Multispectral 4D imaging of Tg(PGK1:H2B-chFP; TIE1:H2B-eYFP) embryo shows assembly of dorsal aortae in the context of the developing ventral trunk region.

Composite movie showing aorta formation in a Tg(PGK1:H2B-chFP; TIE1:H2B-eYFP) double transgenic quail embryo with all cell nuclei (magenta) and EC nuclei (yellow) concomitantly with descent of the AIP. Confocal microscopy of forming dorsal aortae from stages 8-11 (longitudinal view).

(A) The first movie segment shows an overlay of the image data for both the PGK1:H2B-chFP; TIE1:H2B-eYFP chFP+/YFP+ cells.

(B) Image data for only the chFP+ cells.

(C) Image data for only the YFP+ ECs. Angioblasts proliferate and migrate to positions of the presumptive DA in the embryo where they integrate primary vascular plexus. The embryo is oriented with the anterior end (A) on the left. Movie corresponds with data in Fig.5A-C.

Ventral view. Lower left scale bar: 150 um; grid scales mark every 200 um along xy axes; time scale in lower right corner; TIE1:H2B-eYFP+ ECs are pseudo-colored yellow; PGK1:H2B-chFP+ cells are pseudo-colored magenta; AIP, anterior intestinal portal; N, notochord; S, somite; DA, dorsal aorta. Lower left 3D arrows indicate that the embryo is oriented with anterior (A) to the left, lateral (L) to the bottom, and dorsal (D) into the page. Microscope metadata same as Movie 6.

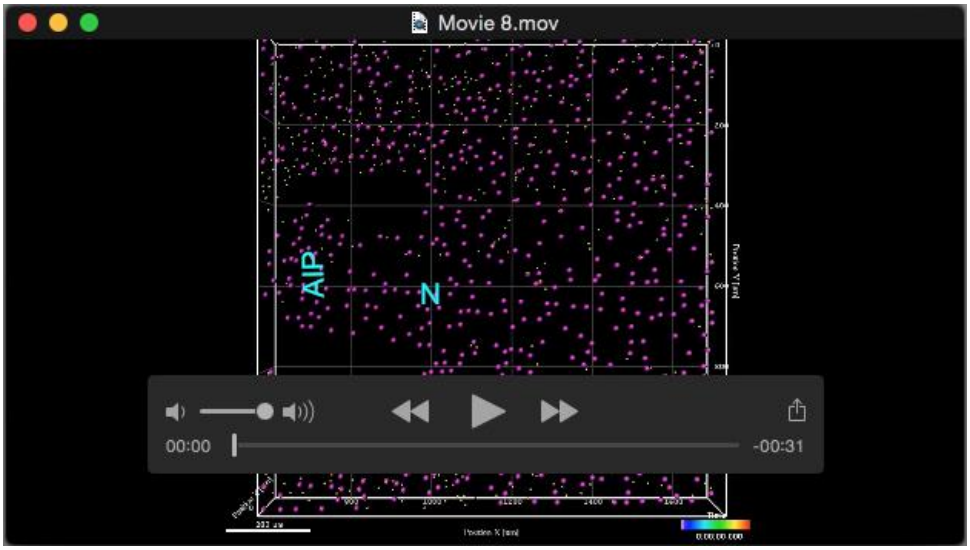

Movie 8. Multispectral 4D cell tracking (*xyzt*) of Tg(PGK1:H2B-chFP) trunk region with focus on dorsal aortae formation.

This movie shows cell-tracking analysis from the image set used to generate Movie 6 and Fig.5. The movie initially shows an overlay of the cell tracking data for both the PGK1:H2B-chFP; TIE1:H2B-eYFP chFP+/YFP+ cells, which is followed by the cell tracking data for only the chFP+ cells, which is followed by the cell tracking data for only the YFP+ ECs. The embryo is oriented with the anterior end (A) on the left. Movie corresponds to data in Fig.5D.

Ventral view. Lower left scale bar: 150 um; grid scales mark every 200 um along xy axes; time scale in lower right corner; TIE1:H2B-eYFP+ ECs are pseudo-colored yellow; PGK1:H2B-chFP+ cells are pseudo-colored magenta; AIP, anterior intestinal portal; N, notochord; DA, dorsal aortae. Lower right 3D arrows indicate that the embryo is oriented with anterior (A) to the left, lateral (L) to the bottom, and dorsal (D) into the page. Microscope metadata same as Movie 6.

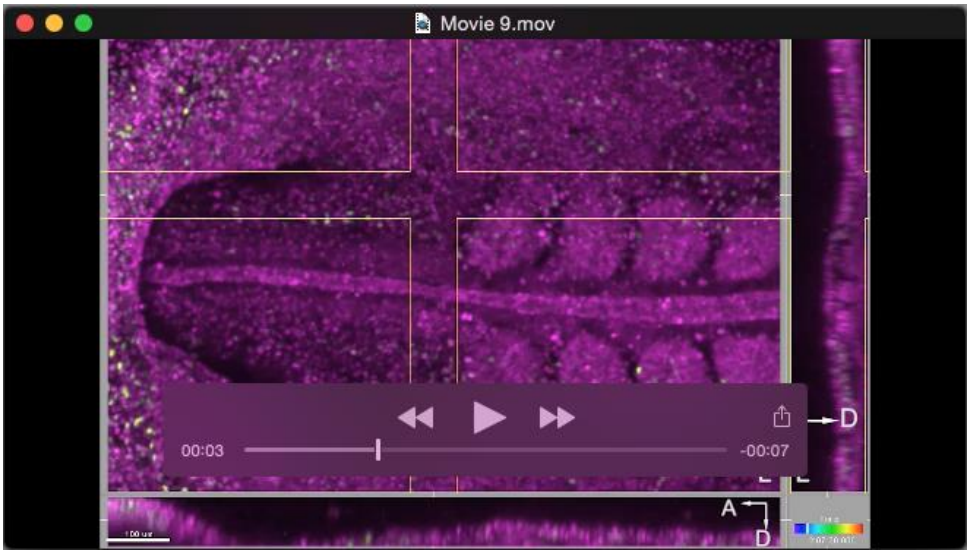

Movie 9. Dorsal aortae formation in 4D.

Confocal microscopy of forming dorsal aortae from stage 8-11 (longitudinal view). The embryo is oriented with the anterior end (A) on the left. This movie shows dorsal aorta formation in 4D from the image set used to generate Movie 6 and Fig.5.

Ventral view. Lower left scale bar: 100 um; time scale in lower right corner; TIE1:H2B-eYFP+ ECs are pseudo-colored yellow; PGK1:H2B-chFP+ cells are pseudo-colored magenta. AIP, anterior intestinal portal; N, notochord; S, somite; DA, dorsal aortae. Arrows indicate how the various slices are oriented for anterior (A), lateral (L), and dorsal (D) directions. Microscope metadata same as Movie 6.

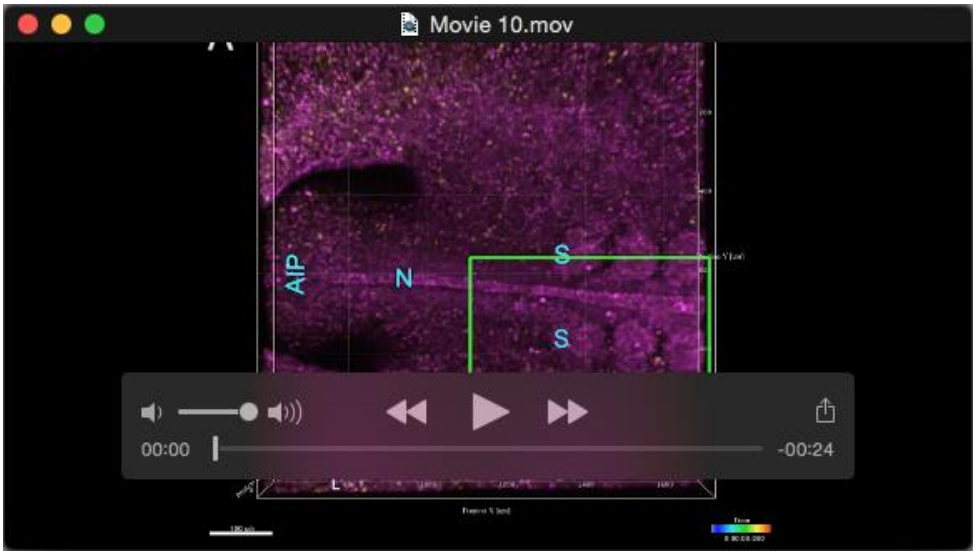

Movie 10. Dorsal aorta formation involves distinct cell behaviors.

A) The green box highlights and defines a higher magnification observation of aorta formation that focuses on EC proliferation, specification, migration and assembly. Putative angioblasts ($chFP^+YFP^-$) can be seen differentiating into ECs ($chFP^+YFP^+$) throughout the movie.

B) Cyan circles surround dividing progenitor cells ($chFP^+YFP^-$), while yellow circles surround representative ROIs of dividing H2B-eYFP+ ECs ($chFP^+YFP^+$) during the first 3 hrs of the movie. Numerous other cell divisions can be seen throughout the movie. The encircled cells quickly move beyond the perimeter of the circles as they collectively move with other embryonic cells during elongation along the A-P axis. Of note are putative angioblasts and ECs within the forming aorta; some of the cells appear to move anterior with the majority of their neighboring aortic cells and thus the general motion of the aorta, whereas other aortic cells continue to move randomly or in a posterior direction, but not anterior.

C) Other tissue specific cells tend to move similar to other cells within their affiliated tissue types as can be viewed within the green oblong: the notochord and adjacent somatic and aortic cells move steadily anterior while a ventral monolayer of putative endoderm cells (marked by white arrow) remain relatively static in terms of A-P motion but not individual motion. Note very bright chFP+ cell near point of arrow at time point 04:30:00 moves anterior at ~100 um/hr, similar to the notochord, somites, dorsal aorta, and adjacent tissue, while the presumptive endoderm cells (7-10 $chFP^+$ cells) remain near the fixed blue arrow.

Ventral view. Lower left scale bar: 70 um; grid scales mark every 200 um along *xy* axes; time scale in lower right corner; TIE1:H2B-$eYFP^+$ ECs are pseudo-colored yellow; PGK1:H2B-$chFP^+$ cells are pseudo-colored magenta; AIP, anterior intestinal portal; N, notochord; S, somite; DA, dorsal aorta. The movie has been slowed down 50%. Lower left 3D arrows indicate that the embryo is oriented with anterior (A) to the left, lateral (L) to the bottom, and dorsal (D) into the page. Microscope metadata same as Movie 6.

References

Chapman, S., Collignon, J., Schoenwolf, G. C. and Lumsden, A. (2001). Improved method for chick whole-embryo culture using a filter paper carrier. *Developmental Dynamics* **220**, 284-289.

Czirok, A., Rupp, P. A., Rongish, B. J. and Little, C. D. (2002). Multi-field 3D scanning light microscopy of early embryogenesis. *J Microsc* **206**, 209-217.

Drake, C. J., Davis, L. A. and Little, C. D. (1992). Antibodies to beta 1-integrins cause alterations of aortic vasculogenesis, in vivo. *Dev Dyn* **193**, 83-91.

Germroth, P. G., Gourdie, R. G. and Thompson, R. P. (1995). Confocal microscopy of thick sections from acrylamide gel embedded embryos. *Microsc Res Tech* **30**, 513-520.

New, D. (1955). A new technique for the cultivation of the chick embryo in vitro. *J Embryol Exp Morphol* **3**, 320-331.

Sato, Y., Poynter, G., Huss, D., Filla, M. B., Czirok, A., Choi, J. M., Rongish, B. J., Little, C. D., Fraser, S. E. and Lansford, R. (2010). Dynamic analysis of vascular morphogenesis using transgenic quail embryos. *PLoS ONE* **5**, e12674.

Warren, M., Puskarczyk, K. and Chapman, S. C. (2009). Chick embryo proliferation studies using EdU labeling. *Dev Dyn* **238**, 944-949.